Quantum Transport in 1D and Quasi-1D Lattice Systems

A Thesis

submitted to

Indian Institute of Science Education and Research Pune

in partial fulfillment of the requirements for the

BS-MS Dual Degree Programme

by

Abhinav Dhawan

Indian Institute of Science Education and Research Pune

Dr. Homi Bhabha Road,

Pashan, Pune 411008, INDIA.

May, 2024

Supervisor: Dr. Bijay Kumar Agarwalla

Certificate

This is to certify that this dissertation entitled Quantum Transport in 1D and Quasi-1D Lattice Systems towards the partial fulfilment of the BS-MS dual degree programme at the Indian Institute of Science Education and Research, Pune represents study/work carried out by Abhinav Dhawan at Indian Institute of Science Education and Research under the supervision of Dr. Bijay Kumar Agarwalla, Associate Professor, Department of Physics , during the academic year 2023-2024.

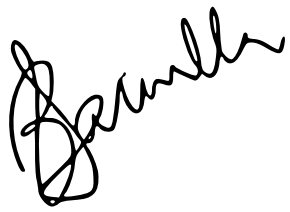

Dr. Bijay Kumar Agarwalla

Committee:

Dr. Bijay Kumar Agarwalla

Dr. Rahul Marathe

This thesis is dedicated to my teachers.

Declaration

I hereby declare that the matter embodied in the report entitled ”Quantum Transport in 1D and Quasi-1D Lattice Systems ” are the results of the work carried out by me at the Department of Physics, Indian Institute of Science Education and Research (IISER) Pune, under the supervision of Dr. Bijay Kumar Agarwalla , and the same has not been submitted elsewhere for any other degree. Wherever others contribute, every effort is made to indicate this clearly, with due reference to the literature and acknowledgment of collaborative research and discussions.

Abhinav Dhawan
Roll No.: 20191121

Acknowledgment

This work is the culmination of a five-year-long journey, which was beautiful and enriching. First and foremost, I want to express my heartfelt gratitude to my family for their love and unwavering support. Each of you has sacrificed for my growth, and we have been together in our joys and hardships. I'm fortunate to have you all. I sincerely thank my advisor, Dr. Bijay Kumar Agarwalla, for patiently guiding me and trusting my abilities, thereby polishing my skills. I must appreciate his serene attitude and a deep passion for research. I thank Dr. Manas Kulkarni and Dr. Madhumita Saha for their valuable input and proactiveness. I am also thankful to Dr. Rahul Marathe for kindly agreeing to be my expert and asking relevant questions during the mid-year evaluation. Discussions with group members were crucial for deepening my understanding, and the credit goes to Katha Ganguly and Sandipan Mohanta. I could unhesitantly ask them any question, big or small, and they were generous with their help. Now comes the Herculean task of acknowledging my pals, where either I write an essay or anonymously thank them all. I conveniently choose the latter. Thank you guys. You have withstood and occasionally participated in the myriads of physics discussions, kept me aware of global and national issues, helped me with coding, and the list is endless. Your company has had a profound impact, and I've definitely learned something or the other from you.

Abstract

This thesis aims to study quantum transport in one-dimensional and quasi one-dimensional lattice systems. The first part deals with non-interacting fermions showing long-range power-law decaying hopping on an open one-dimensional lattice subjected to dephasing noise. Firstly, the steady-state transport driven by boundary baths has been explored by finding the scaling of current with system size. Subsequently, time dynamics is studied by investigating wave-packet spreading. Both of these help to classify transport in the system. Universal super-diffusive transport is observed in the numerical simulations. Analytical calculations support the results obtained. The next part of the thesis deals with ladder set-ups, which are quasi one-dimensional systems. Fermionic transport has been studied in primarily two set-ups: (i) symmetric hopping in the ladder in the presence of a gauge field and (ii) asymmetric hopping in the two legs of the ladder. Transfer matrices and their exceptional points have been studied owing to their connection with transport, and previously known relations in one dimension are generalized to a ladder set-up. A transport-based phase diagram with the phase boundaries corresponding to the exceptional points has been obtained.

Contents

Introduction

Thermodynamics is the study of systems with a large number of degrees of freedom. An equilibrium state has all the macroscopic observables at a steady value with vanishing fluctuations in the thermodynamic limit. A small number of state variables like internal energy, temperature, pressure, entropy, etc completely describe the macrostate. Left to themselves, generic chaotic systems (usually) relax to an equilibrium state, forgetting their initial condition. An equation of state relates state variables of a system, describing the system in a given *thermodynamic phase*. All of this comes under equilibrium thermodynamics. Non-equilibrium thermodynamics, as the name suggests, aims to describe a system that isn't in equilibrium. For instance, a system relaxing to an equilibrium state is essentially a non-equilibrium system, although describing such a system, in general, is a difficult problem. Therefore, for simplicity, one tends to describe systems *near equilibrium* where linear response theory might be applicable. Another class of non-equilibrium systems includes *steady states*. Here, a steady macroscopic current flows through the system by virtue of some gradient, but all the physical observables are at steady time-independent values. For instance, consider an iron rod with two ends subjected to different temperatures. Provided that the boundary temperatures are fixed by some large baths, the rod will develop a steady heat current very soon, flowing from the hot end to the cold end. These non-equilibrium steady states (NESS) are essential for understanding transport phenomena in the system. Transport is described by some equations, such as the diffusion equation, and is associated with transport coefficients like diffusivity, heat conductivity, etc.

One can also study similar notions in quantum systems, which comes under *Quantum Thermo-*

dynamics. Quantum systems are unique because of the possibility of coherence and entanglement. Understanding quantum systems is crucial to fuel advancement in quantum technologies. Real quantum systems can't be isolated from the environment, leading to *dissipation* and *decoherence*. This is a major challenge in quantum computing, demanding a good understanding of *open quantum systems* to prolong or optimally manage it. However, it must be mentioned that dissipation isn't always a problem; for instance, the environment enhances transport in otherwise no-transport regimes [1–3]. Quantum transport is an essential part of non-equilibrium quantum thermodynamics and involves the transport of particles, energy, magnetization, etc, driven by the gradient provided by the boundary baths. A prototypical setup for studying quantum transport involves the central system of interest described by the Hamiltonian H_S, coupled to baths at its left and right ends via coupling Hamiltonians H_{SL} and H_{SR} respectively, as shown in the Fig. 1. The baths are themselves described by their Hamiltonians H_L and H_R. This describes a boundary-driven system, and the total Hamiltonian describes the full system:

$$H = H_S + H_L + H_R + H_{SL} + H_{SR}$$

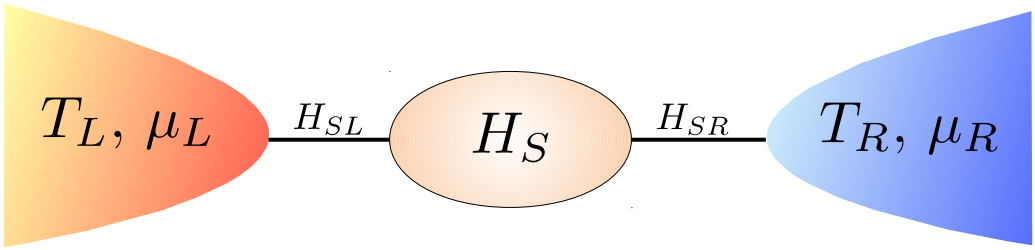

Figure 1: A schematic diagram of a boundary-driven open system

The system's Hamiltonian could contain interactions, coupling with baths could be non-linear, etc. Moreover, the system could be periodically driven, which would break the conservation of energy. All these lead to interesting transport steady states, but can usually be only approximately solved. In this thesis, we will mainly concern ourselves with non-interacting system Hamiltonians. It is found that these can also be very interesting due to the interplay of coherence in the system and the dissipation by the environment. Understanding the simpler case is essential to move on

to complicated cases. The system could also be coupled to multiple baths, and this case is also investigated.

This thesis is organized as follows. In **Chapter 1**, we briefly discuss some preliminaries to provide some background. In **Chapter 2**, the non-equilibrium Green's function (NEGF) technique is used to calculate conductance for a noisy long-range hopping one-dimensional setup driven by boundary baths. In **Chapter 3**, the Lindblad master equation approach is used to model the dephasing probes, and the spread of excitation is studied. A derivation for the fractional diffusion equation [4] describing the anomalous transport in the system is presented. In **Chapter 4**, we calculate conductance for various ladder setups and derive an analytical formula in terms of the transfer matrix. In **Chapter 5**, we conclude by presenting a summary of the main results of the work.

Chapter 1

Preliminaries

Here, I will briefly introduce some important concepts and formulas that will be frequently used afterwards in the thesis. In the first section, we discuss the Landauer-Buttiker formalism, which is useful for studying transport in mesoscopic systems, where the quantum effects are important. Next, we briefly discuss the construction of transfer matrices and some of their basic properties.

1.1 Landauer-Buttiker Formalism

The Landauer-Buttiker formalism relates a system's conductance to the transmission which is a local property [5]. We will be dealing with a non-interacting system, but a generalization for the interacting case exists [5]. The analytical derivation of the formula is derived in terms of non-equilibrium Green's functions, using the equation of motion approach [6]. We first discuss the Landauer formula, which is applicable when the system is coupled to two boundary baths. Then, we discuss the Landauer-Buttiker formula where multiple baths are connected to the system.

1.1.1 Landauer Formula

Consider an open system as shown in Fig. 1. The non-equilibrium steady state (NESS) fermionic current is given by:

$$\mathscr{I} = \int \frac{d\omega}{2\pi} \mathscr{T}(\omega)[f_L(\omega) - f_R(\omega)] \tag{1.1}$$

Here, we consider spinless fermions, and there is a factor of $\frac{e}{\hbar}$ multiplying the above expression but is set to 1 because we set $e = \hbar = 1$. $\mathscr{T}$ is known as the transmission function and given by $\mathscr{T}(\omega) = Tr[G^r(\omega)\Gamma_L(\omega)G^a(\omega)\Gamma_R(\omega)]$ and

$$G^{r/a}(\omega) = \frac{1}{\omega - H_S - \Sigma_L^{r/a} - \Sigma_R^{r/a}} \tag{1.2}$$

are the retarded/advanced Green's functions of the system in the presence of baths. The retarded/advanced self energies $\Sigma_{L/R}^{r/a}(\omega)$ and the bath spectral density functions $\Gamma_{L/R}(\omega)$ are given by:

$$\Sigma_{L/R}^{r/a}(\omega) = H_{SL/SR} g_{L/R}^{r/a}(\omega) H_{SL/SR}^{\dagger} \tag{1.3}$$

$$\Gamma_{L/R}(\omega) = i(\Sigma_{L/R}^{r}(\omega) - \Sigma_{L/R}^{a}(\omega)) \tag{1.4}$$

Here, $g_{L/R}^{r/a}$ is the retarded/advanced Green's function for the isolated bath. The Fermi-Dirac distribution gives the average occupation of the left or right bath $f_{L/R}(\omega)$ as we study fermionic transport. This takes into account the chemical potential $\mu_{L/R}$ and the temperature $T_{L/R}$ of the boundary baths.

When calculating current exactly via the NEGF approach described above, we will mostly be concerned with the zero temperature conductance in the linear response regime unless stated otherwise. This leads to several simplifications as discussed below [7]. Firstly, assuming that only the two boundary sites are connected to the reservoir, say site 1 and M, we have the transmission function simplified to

$$\mathscr{T}(\omega) = \Gamma_L(\omega)\Gamma_R(\omega)\left|G_{1,M}^r(\omega)\right|^2 \tag{1.5}$$

Now, taking zero temperature, we get a simplified form for the average occupation, giving:

$$\mathscr{I} = \int_{\mu_L}^{\mu_R} \frac{d\omega}{2\pi} \mathscr{T}(\omega) \tag{1.6}$$

Furthermore, taking the linear response assumption with $\mu_L = \mu$ and $\mu_R = \mu - d\mu$, we get the conductance $\mathscr{G} = \mathscr{I}/\Delta V$ where $\Delta V = \frac{\mu_L - \mu_R}{e}$, as:

$$\mathscr{G}(\mu) = \mathscr{G}_0 \mathscr{T}(\mu) = \mathscr{G}_0 \Gamma_L(\mu) \Gamma_R(\mu) \left| G^r_{1,M}(\mu) \right|^2 \tag{1.7}$$

where $\mathscr{G}_0 = e^2/2\pi\hbar = 1/2\pi$ is the universal quantum conductance. We will take the wide-band limit for the self-energy unless stated otherwise, making the spectral density functions $\Gamma_{L/R}(\omega)$ independent of ω, i.e., $\Gamma_{L/R}(\omega) = \gamma_{L/R}$.

1.1.2 Landauer-Buttiker Formula

We will now discuss a more general case where the system is connected to multiple baths. Now, we can index the baths, and the average current flowing out of bath ν is given by [8]:

$$\mathscr{I}_\nu = \sum_\alpha \int \frac{d\omega}{2\pi} \mathscr{T}_{\nu\alpha}(\omega) [f_\nu(\omega) - f_\alpha(\omega)] \tag{1.8}$$

Now, the transmission function is given by $\mathscr{T}_{\nu\alpha}(\omega) = Tr[G^r(\omega)\Gamma_\nu(\omega)G^a(\omega)\Gamma_\alpha(\omega)]$, and $f_\nu(\omega) = \left(1 + e^{\beta_\nu(\omega - \mu_\nu)}\right)^{-1}$ is the occupation of the ν-th bath, and

$$G^{r/a}(\omega) = \frac{1}{\omega - H_S - \sum_\alpha \Sigma^{r/a}_\alpha} \tag{1.9}$$

are the retarded/advanced Green's functions of the system in the presence of baths.

We will be concerned with a specific situation where all the sites are connected to dephasing Buttiker voltage probes in addition to the boundary baths. The Buttiker probes can be modeled as baths in a self-consistent state such that no average current flows into them in a steady state. Let the

coupling with the boundary baths be $\gamma_{L/R}$, and let there be uniform coupling of γ_p with the Buttiker probes. The exact solution in the linear response regime is provided in [3] and the conductance is given in terms of $\mathscr{W}$ matrix given by:

$$\mathscr{W} = \begin{pmatrix} \sum_{\alpha\neq 1}\int_{-\infty}^{\infty}\mathscr{T}_{1\alpha}(\varepsilon)\left(-\frac{\partial f_{\rm eq}(\varepsilon)}{\partial\varepsilon}\right)d\varepsilon & -\int_{-\infty}^{\infty}\mathscr{T}_{12}(\varepsilon)\left(-\frac{\partial f_{\rm eq}(\varepsilon)}{\partial\varepsilon}\right)d\varepsilon & -\int_{-\infty}^{\infty}\mathscr{T}_{13}(\varepsilon)\left(-\frac{\partial f_{\rm eq}(\varepsilon)}{\partial\varepsilon}\right)d\varepsilon & \dots \\ -\int_{-\infty}^{\infty}\mathscr{T}_{21}(\varepsilon)\left(-\frac{\partial f_{\rm eq}(\varepsilon)}{\partial\varepsilon}\right)d\varepsilon & \sum_{\alpha\neq 2}\int_{-\infty}^{\infty}\mathscr{T}_{2\alpha}(\varepsilon)\left(-\frac{\partial f_{\rm eq}(\varepsilon)}{\partial\varepsilon}\right)d\varepsilon & -\int_{-\infty}^{\infty}\mathscr{T}_{23}(\varepsilon)\left(-\frac{\partial f_{\rm eq}(\varepsilon)}{\partial\varepsilon}\right)d\varepsilon & \dots \\ -\int_{-\infty}^{\infty}\mathscr{T}_{31}(\varepsilon)\left(-\frac{\partial f_{\rm eq}(\varepsilon)}{\partial\varepsilon}\right)d\varepsilon & -\int_{-\infty}^{\infty}\mathscr{T}_{32}(\varepsilon)\left(-\frac{\partial f_{\rm eq}(\varepsilon)}{\partial\varepsilon}\right)d\varepsilon & \sum_{\alpha\neq 3}\int_{-\infty}^{\infty}\mathscr{T}_{3\alpha}(\varepsilon)\left(-\frac{\partial f_{\rm eq}(\varepsilon)}{\partial\varepsilon}\right)d\varepsilon & \dots \\ \dots & \dots & \dots & \dots \end{pmatrix} \tag{1.10}$$

Setting the temperature of the boundary baths and the probes to zero simplifies the form of $\mathscr{W}$ matrix as follows:

$$\mathscr{W} = \begin{pmatrix} \sum_{\alpha\neq 1}\mathscr{T}_{1\alpha}(\mu) & -\mathscr{T}_{12}(\mu) & -\mathscr{T}_{13}(\mu) & \dots \\ -\mathscr{T}_{21}(\mu) & \sum_{\alpha\neq 2}\mathscr{T}_{2\alpha}(\mu) & -\mathscr{T}_{23}(\mu) & \dots \\ -\mathscr{T}_{31}(\mu) & -\mathscr{T}_{32}(\mu) & \sum_{\alpha\neq 3}\mathscr{T}_{3\alpha}(\mu) & \dots \\ \dots & \dots & \dots & \dots \end{pmatrix} \tag{1.11}$$

The conductance is then given by $\mathscr{G}(\mu) = \mathscr{G}_0\mathscr{T}_{eff}(\mu)$, where the effective transmission function is:

$$\mathscr{T}_{eff}(\mu) = \mathscr{T}_{RL}(\mu) + \sum_{nj}\mathscr{T}_{Rn}(\mu)\mathscr{W}^{-1}_{nj}\mathscr{T}_{jL}(\mu) \tag{1.12}$$

The Buttiker probes effectively mimic the incoherent dephasing effects present in the system due to coupling with the environment or interactions in the system.

1.2 Transfer Matrices

In this section, we'll introduce transfer matrices and their basic properties. Given a Hamiltonian, one can construct the transfer matrix corresponding to it, which is a non-Hermitian matrix, having pseudo-Hermitian property, i.e., its eigenvalues are either purely real or occur as complex conjugate pair(s). This comes from the anti-linear nature of the transfer matrix [9].

There is a deep connection between the spectrum of the Hamiltonian and the eigenvalues of the transfer matrix, which will be explained in Section 4.2. To illustrate the construction of a transfer

matrix, consider a simple fermionic nearest neighbor tight-binding Hamiltonian:

$$H = -t \sum_{m=1}^{N-1} c_m^\dagger c_{m+1} + h.c. \tag{1.13}$$

Let $\begin{pmatrix} \psi_1 & \psi_2 & \cdots \psi_N \end{pmatrix}^T$ denote the energy eigenstate in site basis. Let the corresponding energy be ε. Then, from the time-independent Schrodinger equation, we have:

$$\varepsilon \psi_n = -t\,\psi_{n+1} - t\,\psi_{n-1} \tag{1.14}$$

$$\implies \psi_{n+1} = -\frac{\varepsilon}{t}\psi_n - \psi_{n-1} \tag{1.15}$$

The above equations can be written in terms of the transfer matrix as follows:

$$\begin{pmatrix} -\varepsilon/t & -1 \\ 1 & 0 \end{pmatrix} \begin{pmatrix} \psi_n \\ \psi_{n-1} \end{pmatrix} = \begin{pmatrix} \psi_{n+1} \\ \psi_n \end{pmatrix} \tag{1.16}$$

An exceptional point (EP) of a matrix is when some of the eigenvectors and the eigenvalues coalesce. This is different from degeneracy, where only the eigenvalues become equal. The order of EP is the number of eigenvectors that coalesce. In our example, for $\varepsilon = \pm 2t$, one gets 2nd order exceptional point. Exceptional points are known to be ubiquitous in many physical problems [10], and we will see their role in quantum transport later.

Chapter 2

Quantum transport in 1D Long-range hopping Lattice

In this chapter, we will study the long-range hopping of fermions in a 1D lattice subjected to dephasing noise. We would first study the non-equilibrium steady state (NESS) due to driving by the boundary baths at zero temperature and in the linear response regime. Landauer-Buttiker formalism is used to calculate the conductance, modeling the dephasing noise via coupling to Buttiker probes. Universal superdiffusive transport is observed for strong coupling to the probes, which crosses over to diffusive transport as a function of the long-range parameter α. This is confirmed by plotting the chemical potential profiles. Subsequently, the transition to super-diffusive scaling is understood by tuning the probe coupling from weak to strong.

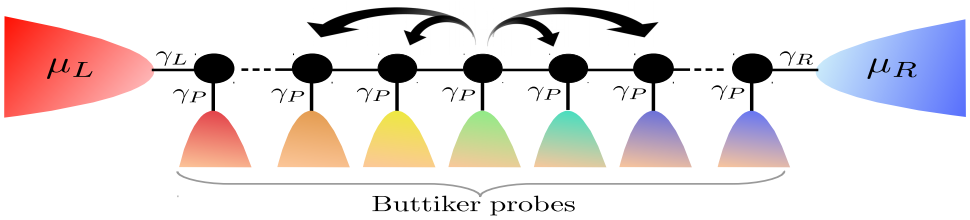

Figure 2.1: A schematic of long-range hopping in a fermionic lattice subjected to dephasing modeled by Buttiker probes connected at each site.

2.1 Long Range Hopping Chain

The Hamiltonian for the long-range hopping lattice chain is given by

$$H_S = -\sum_{m=1}^{N}\sum_{r=1}^{N-m}\frac{1}{m^{\alpha}}c_r^{\dagger}c_{r+m} + h.c. \tag{2.1}$$

where α is the long-range exponent. Here $c_r^{\dagger}$ is the fermionic creation operator at the r-th site, and c_r is the annihilation operator. The above Hamiltonian can be diagonalized assuming periodic boundary condition/taking thermodynamic limit, by going to the Fourier space defining operators $c_k^{\dagger}$ and c_k. Here, we can prove that:

$$\sum_r c_r^{\dagger}c_{r+m} = \sum_k e^{ikm}c_k^{\dagger}c_k \tag{2.2}$$

We finally get the dispersion relation as:

$$\varepsilon(k,\alpha) = -2\sum_{m=1}^{\infty} m^{-\alpha}cos(mk) \tag{2.3}$$

The above is convergent for all k for $\alpha > 1$. The lower and upper band edges are given by Riemann's zeta function and Dirichlet's eta function. [7]

Buttiker dephasing probes are connected to each site of this chain, in addition to the boundary baths attached to the ends of the chain as schematically shown in Fig. 2.1. The linear response conductance is calculated using the Landauer-Buttiker formalism.

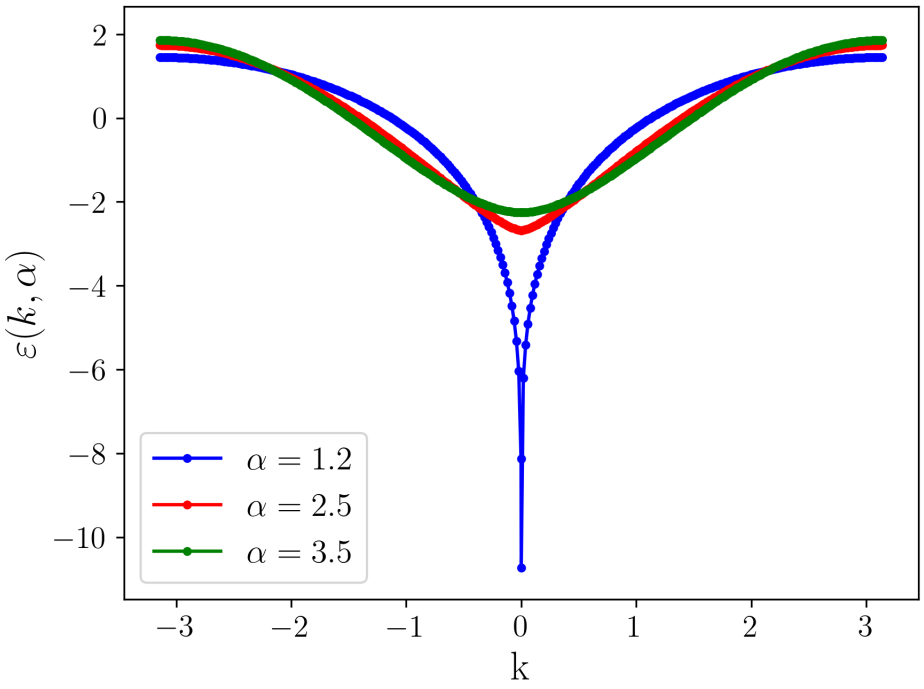

Figure 2.2: Figure for the lattice dispersion relation as given in Eq. 2.3 for different values of long-range exponent α.

First, we would look at the system size scaling of conductance at large system sizes for strong coupling to the probes. Here, due to the extensive broadening of the energy levels, we get a universal scaling exponent independent of the chemical potential of the boundary baths, depending only on the long-range parameter α.

2.2 Strong Probe Coupling

For $\alpha \lesssim 1.5$, a super-diffusive scaling is observed for conductance for large N for sufficiently high coupling with the probes. A crossover to diffusive scaling is observed for $\alpha > 1.5$, making it an effectively short-ranged model. This is shown by the plot below (Fig. 2.3), which was obtained by numerically simulating the conductance given by the Landauer-Buttiker formula. The plot includes two γ_p values, 100 and 1000, for comparison. The scaling is very nearly independent of μ; hence,

when plotting, an average is taken over some chosen μ values. I have also plotted the error bars using the standard deviation about the average. It is observed that the error bars nearly vanish for $\gamma_p = 1000$. Also, even for $\gamma_p = 100$, error bars are found to rapidly decrease as α increases. This could be because of a reduction of the bandwidth of the system's spectrum as alpha increases, leading to less variation with μ. In summary, the universal α dependent super-diffusive exponent is realized for strong coupling to the probes.

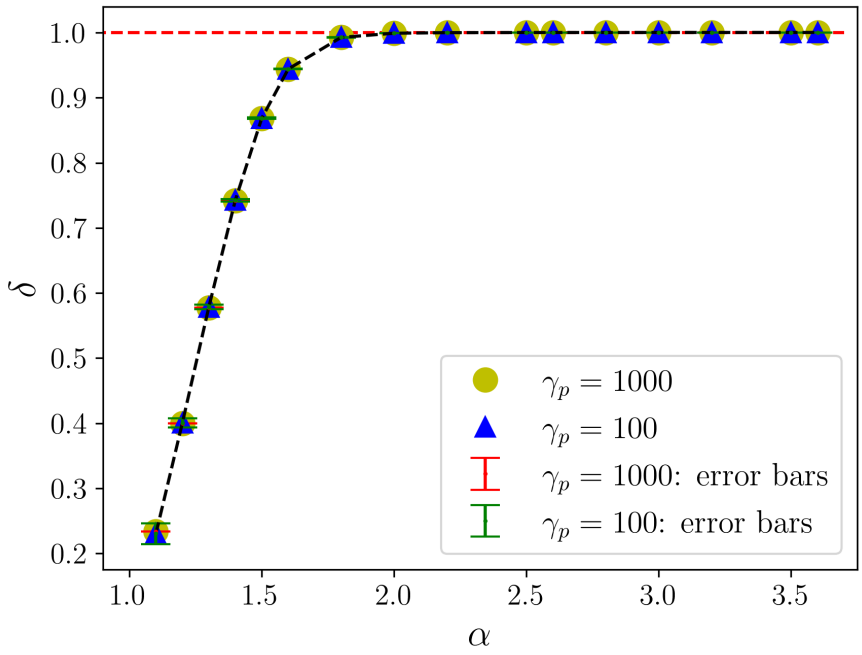

Figure 2.3: The transition from superdiffusive to diffusive regime as α is increased for $\gamma_p = 100, 1000$. The Conductance $\mathscr{G} \sim N^{-\delta}$ (N upto 5431) and $\gamma = 1$ (same for left and right baths). Average is taken with selected μ spanning the whole band, and error bars tell the standard deviation.

.

To investigate the critical α_c, beyond which transport becomes diffusive, we went for larger system sizes (upto $N = 16384$). The results are as tabulated below:

α	μ	$N = 5431$	$N = 16384$	α	μ	$N = 5431$	$N = 16384$
1.1	-20.67	0.2334684435	0.2279934851	2.2	-2.48	0.9999260341	0.9999629184
1.2	-10.68	0.3995437221	0.3993140798	2.5	-2.18	1.000149493	1.000071058
1.3	-7.36	0.5774845175	0.5825519394	2.6	-2.11	1.000174544	1.000082984
1.4	-5.71	0.7418660491	0.7518811974	2.8	-1.99	1.000204027	1.000097007
1.5	-4.72	0.8681394736	0.8805219208	3	-1.90	1.000220011	1.000104605
1.6	-4.07	0.9439254188	0.9539299171	3.2	-1.83	1.000229528	1.000109126
1.8	-3.26	0.9926762827	0.995305777	3.5	-1.75	1.000237732	1.000113024
2	-2.79	0.9990618455	0.9995024461	3.6	-1.73	1.000239521	1.000113871

Table 2.1: Comparizon of $\alpha - \delta$ plot data for system sizes upto 5431 and 16384. μ is taken to be 0.5 above the respective lower band-edge and $\gamma_p = 1000$

From the table, $\delta \approx 2 - 2\alpha$ for $\alpha < 1.5$. This is a surprisingly simple relation. We plot this line along with more data points in Fig. 2.4.

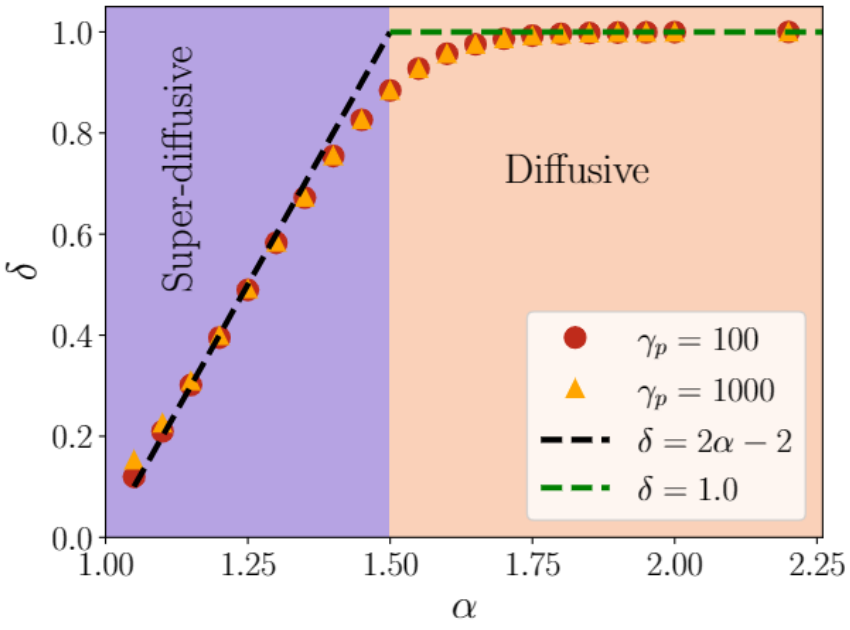

Figure 2.4: $\alpha - \delta$ plot with $\gamma_p = 100, 1000$, and δ is extracted by computing conductance for three large system sizes, $N = 8192$, 11585 and $N = 16384$. with μ taken 0.5 above the lower band edge. The predicted linear relation for $\alpha < 1.5$ shows close agreement with numerical results.

2.3 Chemical Potential Profile

To ascertain superdiffusive behavior, we calculate the local chemical potential of the Buttiker probes in the steady state. This controls the number density at each site. The shape of the profile gives useful information about the nature of transport. We find clear super-diffusive profile for $\alpha = 1.2$, and diffusive profiles for $\alpha = 2.5$ and $\alpha = 3.5$

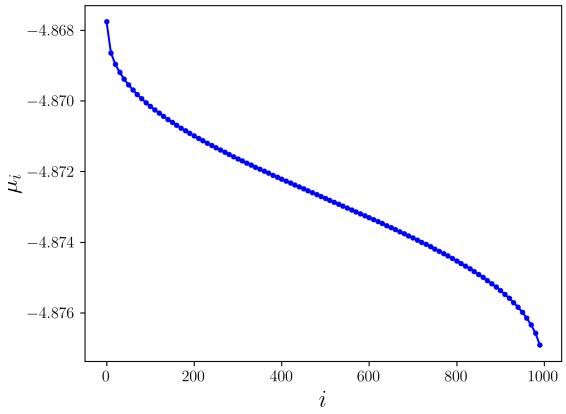

(a) $\alpha = 1.2$

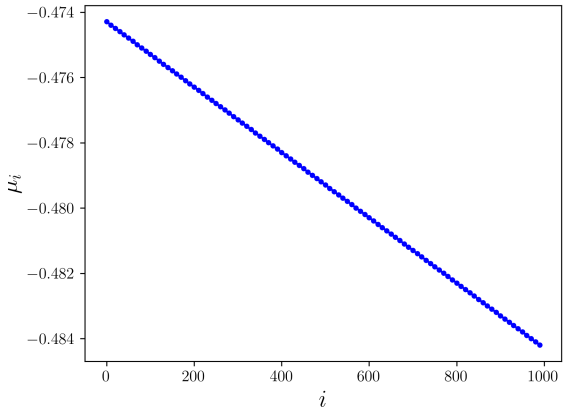

(b) $\alpha = 2.5$

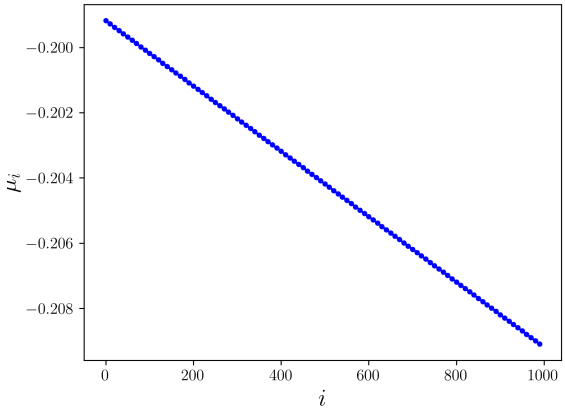

(c) $\alpha = 3.5$

Figure 2.5: Chemical potential profile for different α values. The system size is $N = 1000$, and μ is chosen to be the middle of the band for all the cases. $\Delta\mu = 0.01$ (linear response). $\gamma_p = 1000$, and $\gamma = 1$, as usual.

2.4 Weak to Strong Probe Coupling

Linear response conductance (at zero temperature) for $\alpha = 1.2, 1.3$ and 1.8 for different μ values is extensively analyzed with γ_p varying from 10^{-3} to 10^4. This is done to understand the eventual approach to a universal $\alpha-$ dependent exponent for strong γ_p.

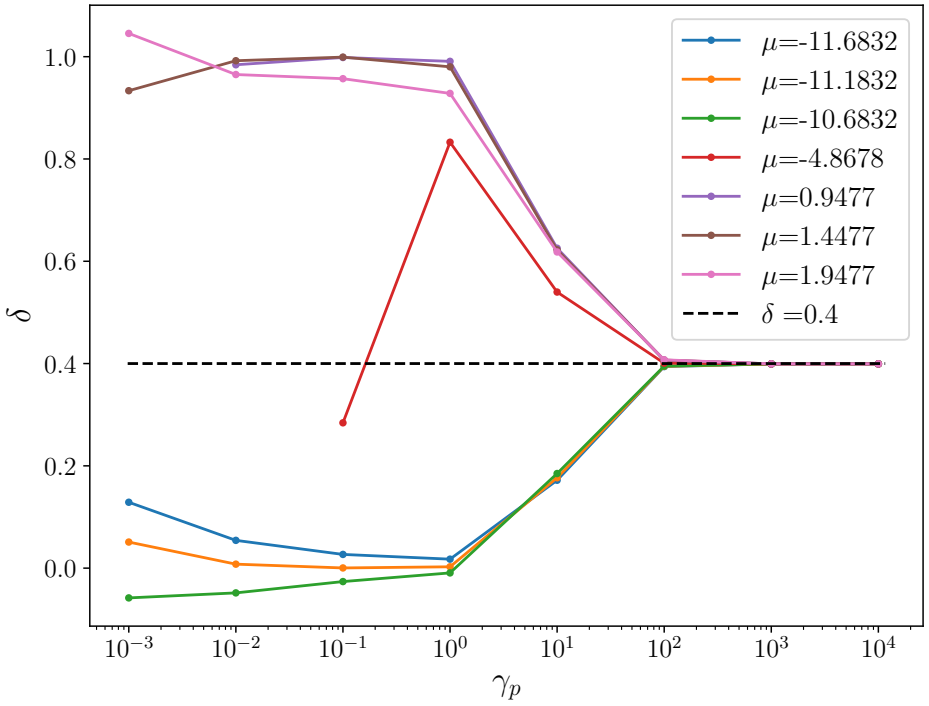

Figure 2.6: The variation of conductance exponent δ for $\alpha = 1.2$ with the probe coupling strength γ_p for chemical potential μ taking 7 values spanning the band. The exponent is extracted by fitting for large N (8192,11585, and 16384 are used). For ballistic behavior due to oscillations, the exponent isn't plotted.

In Fig. 2.6, we clearly see that for $\alpha = 1.2$, the conductance exponent δ becomes universally 0.4, for γ_p greater than 100. It is interesting to note that for μ close to the lower band edge, there is a ballistic to super-diffusive crossover. In contrast, for μ close to the upper band edge, we observe a diffusive to super-diffusive crossover. This suggests the distinct nature of the two band edges. We notice a weak superballistic conductance scaling for μ close to the lower band edge (0.5 above

it). This is discussed in the next section.

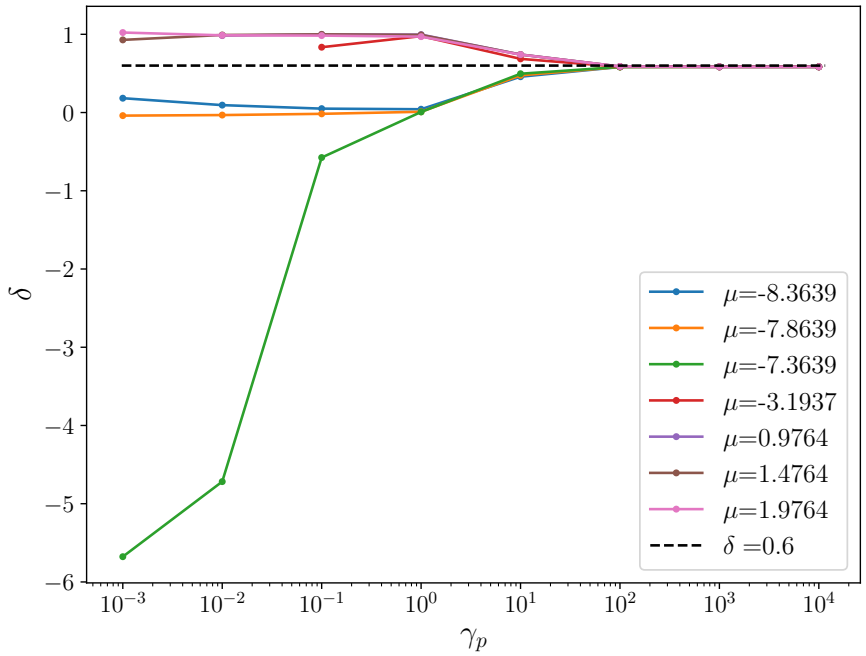

Figure 2.7: The variation of conductance exponent δ for $\alpha = 1.3$ with the probe coupling strength γ_p. The methodology is same as Fig. 2.6

In Fig. 2.7, we have a plot for $\alpha = 1.3$. Here, except for a prominent superballistic behavior, which is discussed later, it is qualitatively similar to the case for $\alpha = 1.2$. The universal exponent at strong coupling is ≈ 0.6.

Fig. 2.8 shows a universal diffusive scaling for strong coupling to the probes. This is expected as we are now in $\alpha > 1.5$ regime, which is effectively short-ranged. However, the superballistic regime is found to be wider for the lower band edge as compared to the upper band edge.

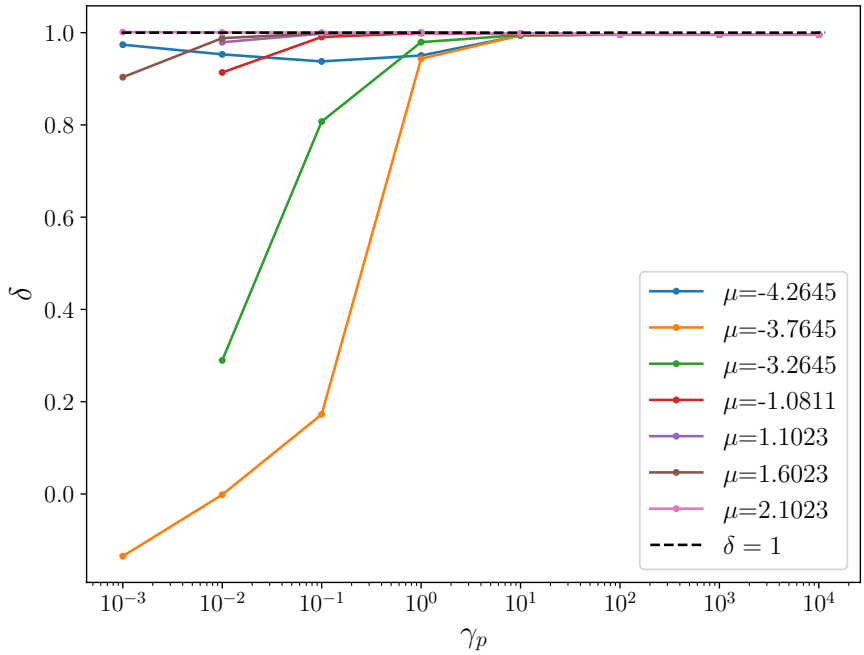

Figure 2.8: The variation of conductance exponent δ for $\alpha = 1.8$ with the probe coupling strength γ_p. The methodology is same as Fig. 2.6

2.4.1 Superballistic scaling at band edges

Short-ranged models are known to host a superballistic regime for intermediate system sizes when the chemical potential of the baths is tuned to the band edge of a system in the presence of weak incoherent effects [11]. The upper band edges, without exception, abide to this rule. Fig. 2.9 shows this for $\alpha = 1.2$.

But for the lower band edge, we don't see a superballistic scaling for $\alpha = 1.2$. However, we see it at the lower band edges at higher α values, such as 2.5 and 3.5. This suggests that some transition is happening as α is decreased. To investigate, more simulations were carried out, with the following results:

For $\alpha = 1.3$, in Fig. 2.10, we see a weak superballistic scaling, but for $\gamma_p = 1$, which is

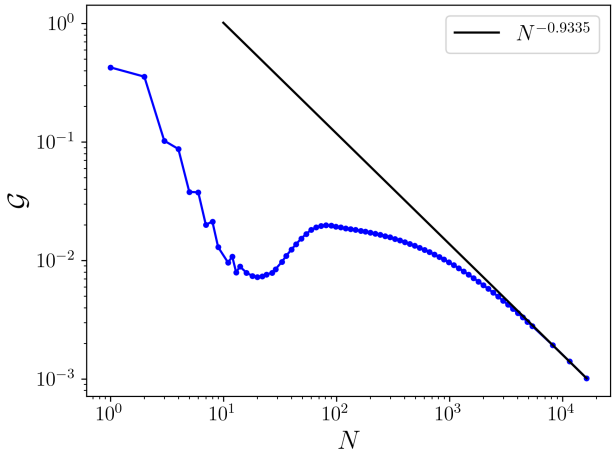

(a) $\gamma_p = 10^{-3}$

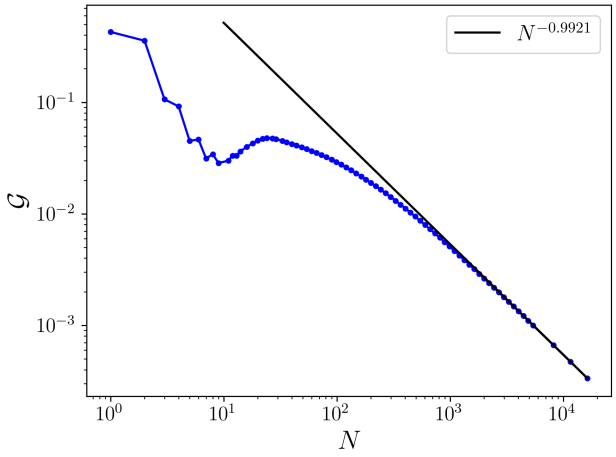

(b) $\gamma_p = 10^{-2}$

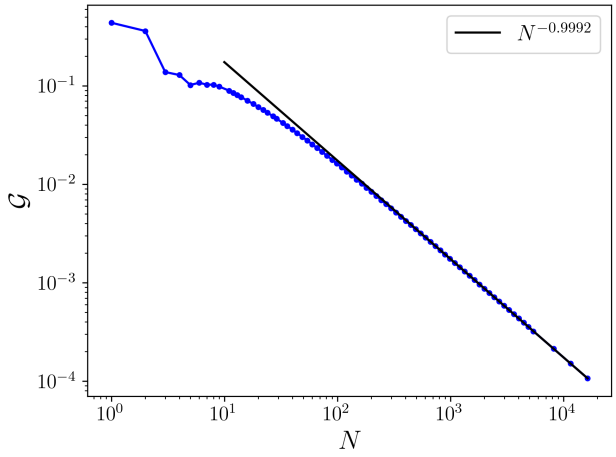

(c) $\gamma_p = 10^{-1}$

Figure 2.9: Log-log plot of conductance with system size showing superballistic scaling at the upper band edge (i.e. $\mu = 1.44765$) for $\alpha = 1.2$ and different values of γ_p. The slope at large N is also indicated.

considerably stronger than the usual probe coupling for observing superballistic scaling. Also, the superballistic scaling is followed by an almost constant conductance (weakly decreasing). If we increase γ_p, the superballistic regime will slowly disappear, and we'll move on toward the universal superdiffusive exponent corresponding to the α value.

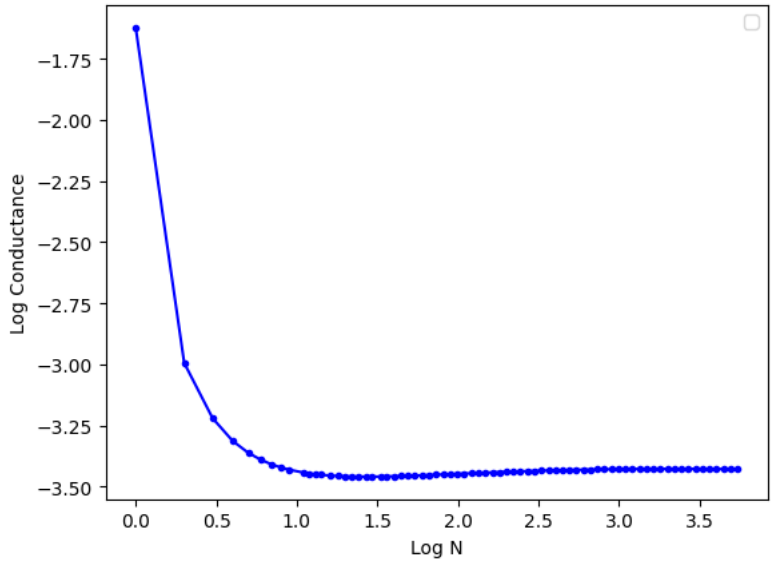

Figure 2.10: Log-log plot for Conductance vs system size $\alpha = 1.3$, μ at lower band edge and $\gamma_p = 1$

Weak superballistic scaling is observed for μ slightly above the lower band edge (i.e. within the band but close to the lower band edge) as shown in Fig. 2.11. We claim that this is not really "superballistic" scaling but rather a late onset of ballistic behavior. To substantiate the claim, the following Fig. 2.12 shows ballistic oscillation after the "superballistic rise" for $\alpha = 1.4$. Therefore, the same can happen for $\alpha = 1.2$, albeit at even larger system sizes.

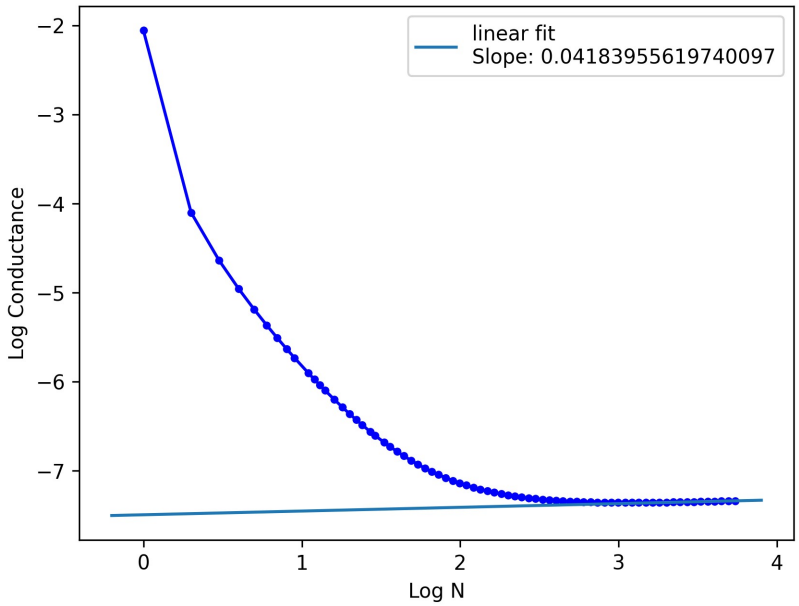

Figure 2.11: Weak super-ballistic scaling above the lower band edge for $\alpha = 1.2$. $\mu = -10.683165$ and $\gamma_p = 10^{-2}$

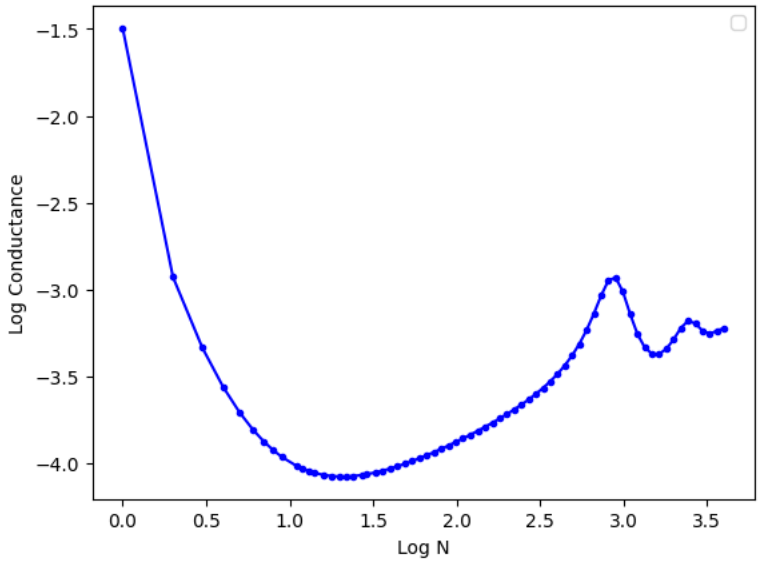

Figure 2.12: Log-log plot of conductance with system size for $\alpha = 1.4$, μ to be 0.5 above lower band edge and $\gamma_p = 0.1$

In summary, it is observed that the transport near the lower band edge is influenced by the transport at the lower band edge, which is subdiffusive ($\sim 1/N^2$). This may be due to the non-analyticity at the lower band edge. It is seen in the following ways.

Firstly, the transport below the lower band edge doesn't quickly go to the value of $N^{-2\alpha}$, as it should. A very large system size is probably needed to realize the expected scaling. Secondly, ballistic behavior is suppressed near the lower band edge within the band edge. This is evident in the initial $1/N^2$ scaling of conductance with N in the plot below. The probes are probably weakening this dependence on the lower band edge. As probe coupling strength is increased, the probes start to steer the transport towards the universal superdiffusive regime.

2.5 Conductance scaling with probe coupling strength

Now, we look at how conductance scales with the strength of the coupling with the Buttiker probes. Note that the simulations are done assuming the wide-band limit. This scaling helps us know about the environment's role in transport.

The scaling is similar to the one obtained for noisy AAH and GAAH models in [3].[1] It is interesting to note that even a long-range model follows the same scaling as a quasi-periodic short-range model.

In large γ_p limit, the conductance goes as $1/\gamma_p^2$, independent of α or μ. This is known as the quantum Zeno effect [12] as shown by the following plot:

[1] In [3], tight-binding self-energy is used, and hence γ_p there is different from the one used by us, but related. When this is considered, the scaling is the same

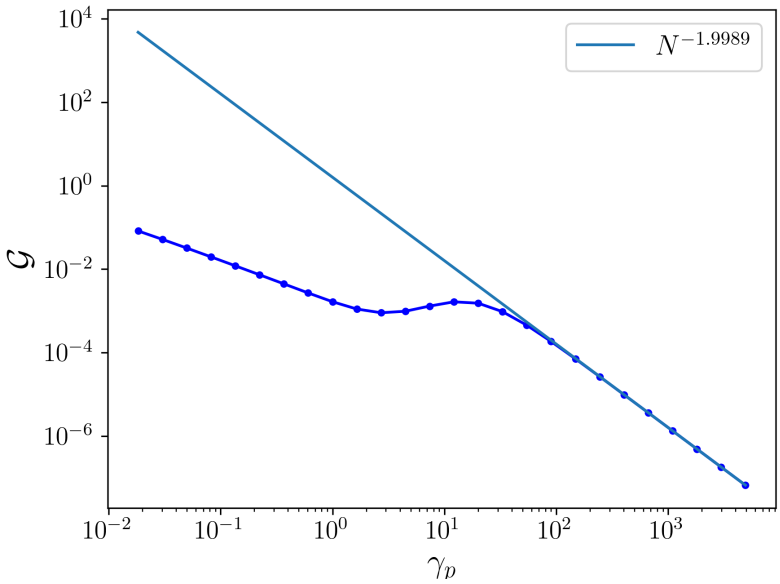

Figure 2.13: A plot showing the conductance scaling with γ_p. The plot is representative of all parameter values, in large γ_p limit. Here, specifically, $N = 1000$, $\mu = 0.91762$, and $\alpha = 1.1$

Scaling for No-transport regimes

It has been found that weak coupling with the probes indeed enhances transport in no-transport regimes [1–3], which here corresponds to μ outside the band. In addition to scaling as $1/\gamma_p^2$ in the large γ_p limit, we find that in the small γ_p limit, the conductance roughly scales as γ_p^2. For $\alpha = 1.2$, the scaling is a bit less than 2. This could again stem from the non-analyticity of the lower band edge. Following are the plots for the three α values:

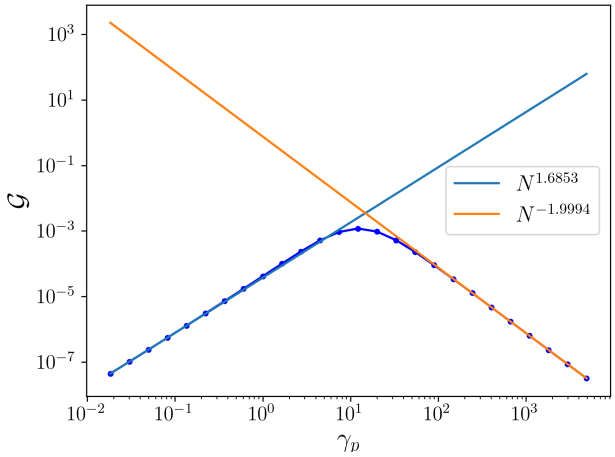

(a) $\alpha = 1.2$

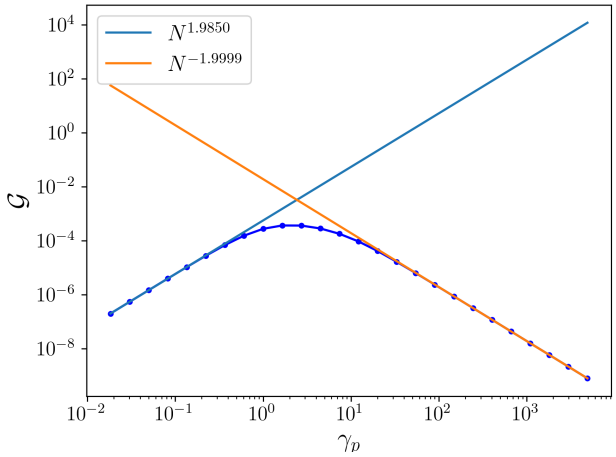

(b) $\alpha = 2.5$

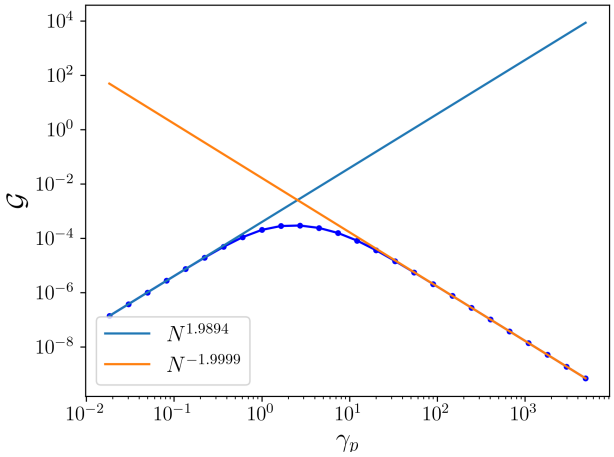

(c) $\alpha = 3.5$

Figure 2.14: Log-Log plot for conductance vs γ_p for different α values in a no-transport regime. The system size is $N = 1000$, and μ is chosen to be 0.5 less than the lower band edge. $\gamma = 1$, as usual.

Chapter 3

Excitation Dynamics in 1D Long-range hopping Lattice

In this chapter, we will look at the same long-range hopping system, but we will model the dephasing by the probes using the Lindblad master equation. It is known to show anomalous superdiffusive transport in the same parameter regime $1 < \alpha < 1.5$, and diffusive transport for larger values of α [13]. We will use unitary unraveling of the master equation to study excitation spreading in the system numerically. Wavepacket dynamics has been used to study transport in other systems as well [14]. The results are presented and subsequently supported by analytical calculations.

Consider the same long-range power-law decaying hopping free fermionic Hamiltonian:

$$H_S = -\sum_{m=1}^{N}\sum_{r=1}^{N-m}\frac{J}{m^{\alpha}}c_i^{\dagger}c_{i+m} + h.c. \tag{3.1}$$

Zeno-type dephasing is added at each site of this chain as shown in Fig. 3.1 We model the system via Lindblad formalism. We will set $J = 1$. The time evolution of the density matrix is given by:

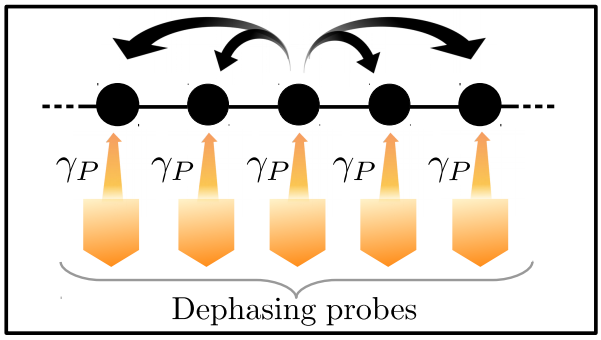

Figure 3.1: A schematic of long-range hopping in a fermionic lattice subjected to Lindblad dephasing.

$$\frac{d\rho(t)}{dt} = -i[H_S, \rho(t)] + \gamma_p \sum_{j=-L/2}^{L/2} \left(n_j \rho(t) n_j - \frac{1}{2}\{n_j^2, \rho(t)\} \right) \tag{3.2}$$

3.1 Unitary Unraveling

The master equation 3.2 describes the evolution of the density matrix, whose dimension is $\mathcal{N}^2$ if $\mathcal{N}$ is the Hilbert space dimension. This becomes very large as the number of sites increases. Therefore, an effective way to numerically simulate such an evolution is by using unitary unraveling [15, 16]. Here, we work with a stochastic Hamiltonian, where the noise takes into account the effect of the environment. Subsequently, we must do an average over all the noise trajectories to extract physical quantities. In the limit of a large number of trajectories, the two approaches can be shown as equivalent.

The time evolution operator is given by:

$$\hat{U}(t+dt,t) = e^{-i\hat{H}dt - i\sqrt{\gamma_p dt}\Sigma_i \eta_i(t)\hat{n}_i} \tag{3.3}$$

Here, $\eta_i(t)$ is delta-correlated Gaussian white noise with unit variance. The time step dt must be less than all the time scales present in the system. For our case, we require $dt \ll min\{J^{-1}, \gamma_p^{-1}\}$;

Consider a one-dimensional lattice of length $N = 2l + 1$ with lattice points from $-l$ to l. We will study the spread of a density excitation. We start with a single particle at the middle site, i.e., at 0, and let the system evolve. Eq. 3.2 doesn't change the number of particles in the system. In this sense, we can understand it as a continuous monitoring of local number density. Also, notice that because the Lindblad jump operators are Hermitian, it can be shown that $\rho_\infty = \frac{1}{\mathcal{N}}\mathbb{1}$ is a steady state, and hence the time dynamics will converge to this state. This is the infinite temperature state, as all the states are equally likely. But, we are interested in the dynamics and not the steady-state solution.

We'll study the time dynamics of the probability distribution. This tells us how the excitations locally relax, which is exactly how a closed system approaches the equilibrium situations. Because our system is discrete, we deal with discrete probability distributions, also known as probability mass functions. It is given by the corresponding element of the single particle propagator, as follows:

$$P(i,t) = \left|U_{i,0}(t,0)\right|^2 \tag{3.4}$$

As mentioned, the probability is obtained by averaging over the probabilities obtained from all the noise trajectories. In the next section, we present the results of the numerics.

3.2 Numerical Results

We simulate the system with the number of lattice points $N = 201$. It is ensured that there are no significant boundary effects by remaining in a time window. Therefore, we consider long times but staying within the window. The regime of transport is found by extracting the spatio-temporal scaling dependence. If $x \sim t^\beta$, then β will tell us about the regime of transport. The probability distribution function will be given by:

$$P(x,t) = (Dt)^{-\beta} K\left(\frac{x}{(Dt)^\beta}\right) \tag{3.5}$$

Here, K is a scaling function dependent only on one variable, namely $x/(Dt)^{\beta}$, and D is a generalized diffusion coefficient. If we accordingly scale the $x-$ and $y-$ axis, we would see a collapse of trajectories at different times for the correct scaling exponent β.

Transport regimes can be identified based on the value of β. $\beta = 1$ holds for ballistic transport, $\beta = 0.5$ for diffusive transport. For $\beta < 0.5$, we are in the sub-diffusive regime, while for $0.5 < \beta < 1$ is the super-diffusive regime (but sub-ballistic). $\beta > 1$ is super-ballistic. Generally, for short-ranged models, a diffusive regime is expected for sufficiently large coupling with the dephasing probes [17, 18]. Now, we will look at the results for the long-ranged model:

The results for $\alpha = 1.2$ and $\alpha = 1.8$ are in the Fig. 3.2 and Fig. 3.3 respectively. We notice that we have a super-diffusive scaling exponent for $\alpha = 1.2$, while a diffusive exponent for $\alpha = 1.8$

A Gaussian scaling function fits the bulk for $\alpha = 1.8$, but heavy tails are observed deviating from the Gaussian function. Also, collapse in the tail is not as good as the bulk. Fig. 3.4 shows the Gaussian fit for the bulk.

3.3 Fractional Diffusion Equation: Microscopic derivation

The high dephasing γ_p in Eq. 3.2 renders the transport classical. Using the renormalization technique [19], we will see how such a classical master equation arises. We will adapt the procedure given in [20].

Consider the equation of motion of $D_{m,n}(t) \equiv \left\langle a_m^{\dagger}(t) a_n(t) \right\rangle$:

$$\frac{d}{dt} D_{m,n}(t) = iJ \sum_{l \neq 0} \left(\frac{D_{m,n+l}(t) - D_{m+l,n}(t)}{|l|^{\alpha}} \right) + \gamma_p \left(\delta_{m,n} - 1 \right) D_{m,n}(t) \tag{3.6}$$

We change the variables to $\tau = \gamma_p t$, and work in the strong dephasing limit i.e., $\gamma_p \gg J$ where

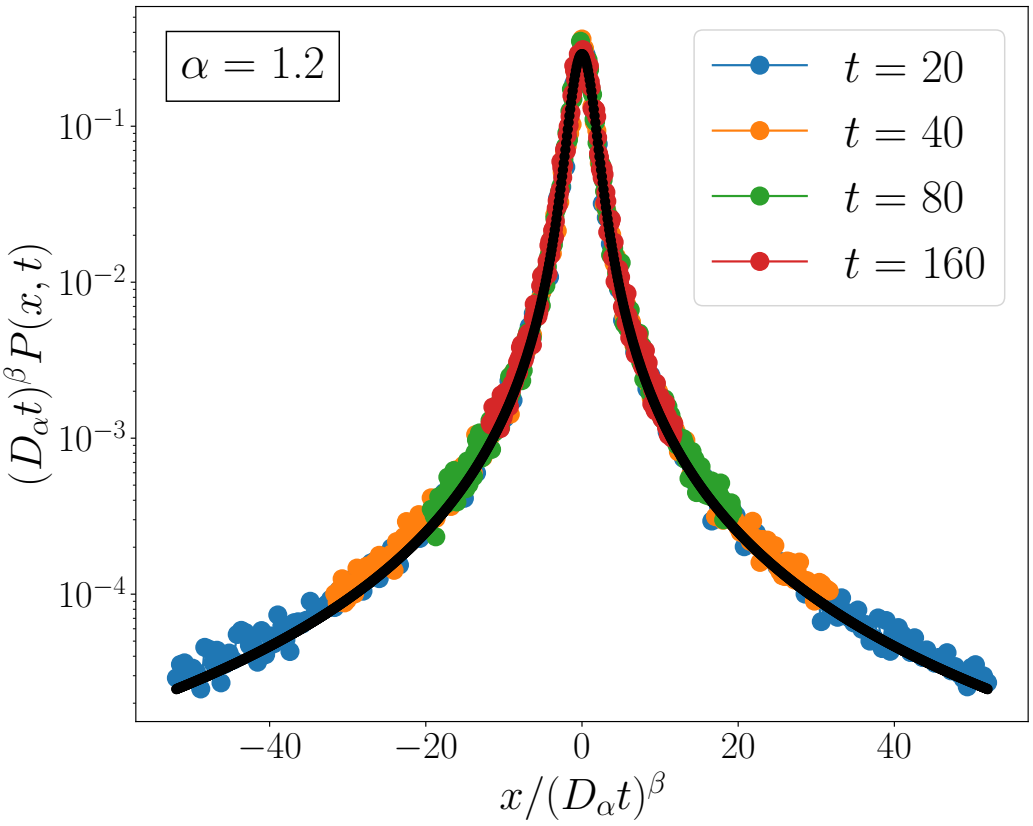

Figure 3.2: Scaling collapse for $\alpha = 1.2$, $\gamma_p = 50$, and $N = 201$ lattice sites. Noise averaging is done over 60 noise trajectories. The black curve is the analytical function fitting the collapse very well. The exponent $\beta = 1/(2\alpha - 1)$ for $1 < \alpha < 1.5$, and the form of D_α is discussed in the text.

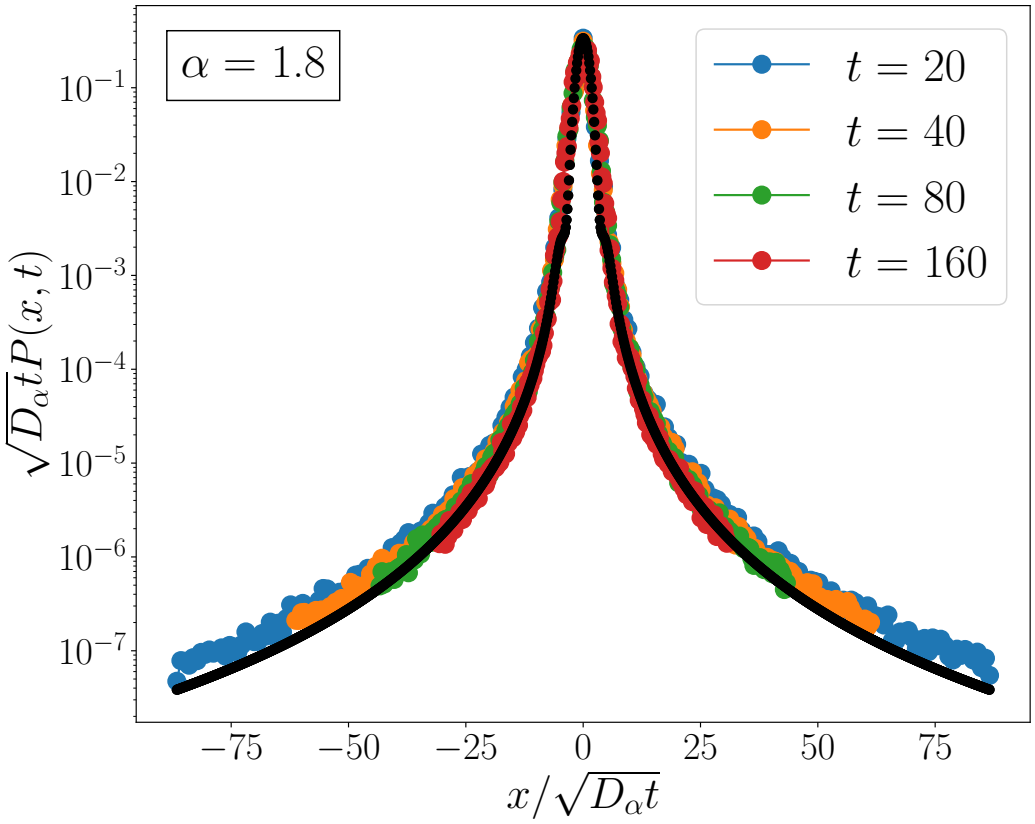

Figure 3.3: Scaling collapse for $\alpha = 1.8$, $\gamma_p = 50$, and $N = 201$ lattice sites. Noise averaging is done over 60 noise trajectories. It is noted that the tails don't collapse with the scaling used, but the bulk shows a diffusive collapse. The analytical function (with corrections) used here is specifically for time $t = 160$, and is elaborated further in the text, along with form for D_α

.

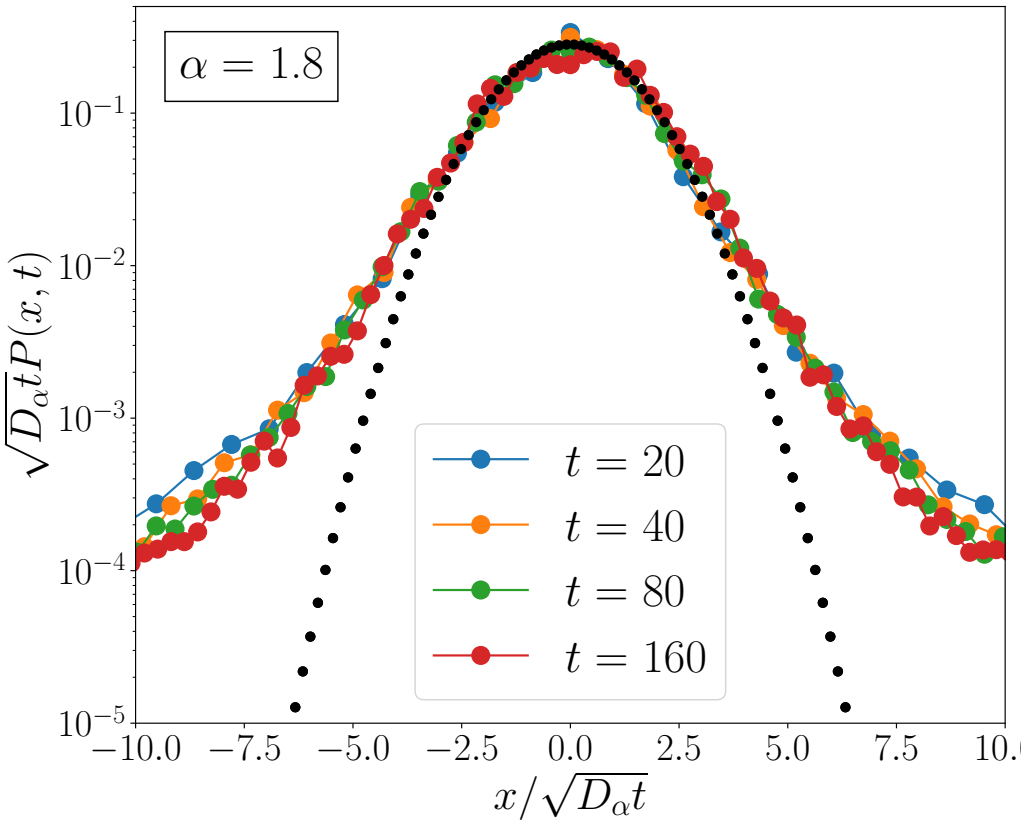

Figure 3.4: Scaling collapse for $\alpha = 1.8$, same as Fig. 3.3. A Gaussian function is found to be a good fit in the bulk. Heavy tails are clearly seen, which are not captured by the Gaussian function and corrections are required, as discussed in the text.

recall that J is the hopping strength. $\varepsilon_l = \frac{J\gamma_p^{-1}}{l^\alpha}$, $l \geq 1$. We will expand in terms of a small parameter

$$\varepsilon = \sum_{l\geq 1} \varepsilon_l, \tag{3.7}$$

which converges for $\alpha > 1$. We then receive,

$$\frac{d}{d\tau} D_{m,n}(\tau) = i \sum_{l\neq 0} \varepsilon_{|l|} \left(D_{m,n+l}(\tau) - D_{m+l,n}(\tau) \right) + \lambda_{m,n} D_{m,n}(\tau) \tag{3.8}$$

where $\lambda_{m,n} = \delta_{m,n} - 1$. Now, expanding $D_{m,n}(\tau)$ in powers of ε, we have

$$D_{m,n}(\tau) = D^{(0)}_{m,n}(\tau) + \varepsilon D^{(1)}_{m,n}(\tau) + \varepsilon^2 D^{(2)}_{m,n}(\tau) + \ldots \tag{3.9}$$

Substituting this in Eq. (3.8), and matching order by order, we get:

$$\frac{d}{d\tau} D^{(0)}_{m,n}(\tau) = \lambda_{m,n} D^{(0)}_{m,n}(\tau) \tag{3.10}$$

$$\varepsilon \frac{d}{d\tau} D^{(1)}_{m,n}(\tau) = \varepsilon \lambda_{m,n} D^{(1)}_{m,n}(\tau) + i \sum_{l\neq 0} \varepsilon_{|l|} \left(D^{(0)}_{m,n+l}(\tau) - D^{(0)}_{m+l,n}(\tau) \right) \tag{3.11}$$

$$\varepsilon^2 \frac{d}{d\tau} D^{(2)}_{m,n}(\tau) = \varepsilon^2 \lambda_{m,n} D^{(2)}_{m,n}(\tau) + i \sum_{l\neq 0} \varepsilon_{|l|} \varepsilon \left(D^{(1)}_{m,n+k}(\tau) - D^{(1)}_{m+k,n}(\tau) \right) \tag{3.12}$$

$$\vdots \tag{3.13}$$

$$\varepsilon^a \frac{d}{d\tau} D^{(a)}_{m,n}(\tau) = \varepsilon^a \lambda_{m,n} D^{(a)}_{m,n}(\tau) + i \sum_{l\neq 0} \varepsilon_{|l|} \varepsilon^{a-1} \left(D^{(a-1)}_{m,n+k}(\tau) - D^{(a-1)}_{m+k,n}(\tau) \right) \tag{3.14}$$

which gives,

$$\frac{d}{d\tau}D^{(0)}_{m,n}(\tau) = \lambda_{m,n}D^{(0)}_{m,n}(\tau) \tag{3.15}$$

$$\frac{d}{d\tau}D^{(1)}_{m,n}(\tau) = \lambda_{m,n}D^{(1)}_{m,n}(\tau) + \frac{i}{\varepsilon}\sum_{l\neq 0}\varepsilon_{|l|}\left(D^{(0)}_{m,n+l}(\tau) - D^{(0)}_{m+l,n}(\tau)\right) \tag{3.16}$$

$$\frac{d}{d\tau}D^{(2)}_{m,n}(\tau) = \lambda_{m,n}D^{(2)}_{m,n}(\tau) + \frac{i}{\varepsilon}\sum_{l\neq 0}\varepsilon_{|l|}\left(D^{(1)}_{m,n+l}(\tau) - D^{(1)}_{m+l,n}(\tau)\right) \tag{3.17}$$

$$\vdots \tag{3.18}$$

$$\frac{d}{d\tau}D^{(a)}_{m,n}(\tau) = \lambda_{m,n}D^{(a)}_{m,n}(\tau) + \frac{i}{\varepsilon}\sum_{l\neq 0}\varepsilon_{|l|}\left(D^{(a-1)}_{m,n+l}(\tau) - D^{(a-1)}_{m+l,n}(\tau)\right) \tag{3.19}$$

Let us now consider the initial condition to be such that $D_{m,n}(\tau=0) = D^{(0)}_{m,n}(\tau=0)$. This makes $D^{(a)}_{m,n}(\tau=0) = 0$ for all $a > 0$. Solving the 0^{th} order equation, we have

$$D^{(0)}_{m,n}(\tau) = A_{m,n}e^{\lambda_{m,n}\tau}, \tag{3.20}$$

$$D^{(1)}_{m,n}(\tau) = \frac{ie^{\lambda_{m,n}\tau}}{\varepsilon}\int_0^\tau dt'\, e^{-\lambda_{m,n}t'}\sum_{l\neq 0}\varepsilon_{|l|}\left(D^{(0)}_{m,n+l}(t') - D^{(0)}_{m+l,n}(t')\right). \tag{3.21}$$

Now, substituting the 0^{th} order solution into 1^{st} order equation, we get for the diagonal and non-diagonal elements of $D^{(1)}_{m,n}(\tau)$ as

$$D^{(1)}_{m,m}(\tau) = \frac{i(1-e^{-\tau})}{\varepsilon}\sum_{l\neq 0}\varepsilon_{|l|}\left(A_{m,m+l} - A_{m+l,m}\right) \tag{3.22}$$

$$\begin{aligned} D^{(1)}_{m,m+b}(\tau) = &\frac{i\tau e^{-\tau}}{\varepsilon}\sum_{l\neq 0,-b}\varepsilon_{|l|}\left(A_{m,m+b+l} - A_{m-l,m+b}\right) \\ &+ \frac{i(1-e^{-\tau})\varepsilon_{|b|}}{\varepsilon}\left(A_{m,m} - A_{m+b,m+b}\right) \end{aligned} \tag{3.23}$$

Now, because we are interested in the populations (upto 2nd order), we focus on $D^{(2)}_{m,m}(\tau)$

$$D^{(2)}_{m,m}(\tau) = \frac{i}{\varepsilon}\int_0^\tau dt' \sum_{l\neq 0} \varepsilon_{|l|}\left(D^{(1)}_{m,m+l}(t') - D^{(1)}_{m+l,m}(t')\right) \tag{3.24}$$

$$= \frac{2\tau}{\varepsilon^2}\sum_{l\neq 0}\varepsilon^2_{|l|}\left(A_{m+l,m+l} - A_{m,m}\right) + (\text{Convergent term in } \tau) \tag{3.25}$$

Therefore, collecting the terms upto the second order, the complete solution for $D_{m,m}$ is given by,

$$\begin{aligned} D_{m,m}(\tau) \approx & A_{m,m} + i(1-e^{-\tau})\sum_{l\neq 0}\varepsilon_{|l|}\left(A_{m,m+l} - A_{m+l,m}\right) \\ & + 2\tau\sum_{l\neq 0}\varepsilon^2_{|l|}\left(A_{m+l,m+l} - A_{m,m}\right) + (\text{Convergent term in } \tau) \end{aligned} \tag{3.26}$$

The first term of the second order term diverges with $\tau \to \infty$. Therefore, we need to cancel the divergence by introducing a parameter τ' and changing $A_{m,m} \to A_{m,m}(\tau')$ and get:

$$\begin{aligned} D'_{m,m}(\tau,\tau') \approx & A_{m,m}(\tau') + i(1-e^{-\tau})\sum_{l\neq 0}\varepsilon_{|l|}\left(A_{m,m+l} - A_{m+l,m}\right) \\ & + 2(\tau-\tau')\sum_{l\neq 0}\varepsilon^2_{|l|}\left(A_{m+l,m+l}(\tau') - A_{m,m}(\tau')\right) \\ & + (\text{Convergent term in } \tau) \end{aligned} \tag{3.27}$$

The condition we impose is:

$$\frac{d}{d\tau'}D'_{m,m}(\tau,\tau')\Big|_{\tau=\tau'} = 0 \tag{3.28}$$

This gives us the following equation for $A_{m,m}(\tau)$:

$$\frac{d}{d\tau}A_{m,m}(\tau) = 2\sum_{l\neq 0}\varepsilon^2_{|l|}\left(A_{m+l,m+l}(\tau) - A_{m,m}(\tau)\right) \tag{3.29}$$

Now, $D_{m,m} = A_{m,m}$ and since $A_{m,m}$ is a function of τ, so is $D_{m,m}$. This gives us the following:

$$\frac{d}{d\tau}D_{m,m}(\tau) = 2\sum_{l\neq 0}\varepsilon^2_{|l|}\left(D_{m+l,m+l}(\tau) - D_{m,m}(\tau)\right) \tag{3.30}$$

Transforming back to the time variable t as $\tau = \gamma_p t$, we get:

$$\frac{d}{dt}D_{m,m}(t) = \frac{2J^2}{\gamma_p}\sum_{l\neq 0}\left(\frac{D_{m+l,m+l}(t) - D_{m,m}(t)}{|l|^{2\alpha}}\right). \tag{3.31}$$

The above is exactly the classical master equation that is phenomenologically argued via Fermi's golden rule [21,22]. This completes a microscopic derivation leading to no phenomenological free parameter. In a continuum, Eq. 3.31 becomes a fractional diffusion equation for some regime of α values, leading to anomalous superdiffusive transport in that regime, as shown in the next section, where we expand on the calculations in Ref. [21].

3.4 Solving the Classical Master Equation

Consider the following general classical master equation describing hard-core particles.

$$\partial_t f_j(t) = \sum_{i\neq j}(W_{i\to j}f_i(1-f_j) - W_{j\to i}f_j(1-f_i)) \tag{3.32}$$

The transition rates $W_{i\to j}$ are determined by the microscopic Hamiltonian via our derivation using renormalization in section 3.3. This gives:

$$W_{i\to j} = W_{j\to i} = \frac{\lambda}{|i-j|^{2\alpha}} \tag{3.33}$$

Here, λ^{-1} is a characteristic time scale determined by the evolution of the system in the presence of probes. As calculated in the previous section $\lambda = \frac{2J^2}{\gamma_p}$

Therefore, now the classical master equation becomes:-

$$\partial_t f_j(t) = \sum_{i\neq j} W_{i\to j}(f_i - f_j) \tag{3.34}$$

Let

$$W(k) = \sum_{i-j=-L/2, i\neq j}^{L/2} e^{-ik(i-j)} W_{i\to j} \tag{3.35}$$

then we have,

$$W_{i\to j} = \frac{1}{L+1} \sum_{k} e^{ik(i-j)} W(k) \tag{3.36}$$

Here, $k = 2\pi n/L$ with $n = -L/2, \cdots, L/2$. Starting with RHS of Eq. 3.34, we get:

$$\sum_{i\neq j} W_{i\to j}(f_i - f_j) = \frac{1}{(L+1)^2} \sum_{i\neq j} \sum_{k,k'} (e^{ik(i-j)} W(k) e^{ik'i} f(k') - e^{ik(i-j)} W(k) e^{ik'j} f(k')) \tag{3.37}$$

$$\implies = \frac{1}{(L+1)^2} \sum_{k,k'} (e^{-ikj} W(k) f(k') \sum_{i\neq j} e^{i(k+k')i} - e^{i(k'-k)j} W(k) f(k') \sum_{i\neq j} e^{iki}) \tag{3.38}$$

$$\implies = \frac{1}{L+1} \sum_{k,k'} (e^{-ikj} W(k) f(k') \delta_{k+k',0} - e^{i(k'-k)j} W(k) f(k') \delta_{k,0}) \tag{3.39}$$

$$\implies = \frac{1}{L+1} (\sum_{k} e^{-ikj} W(k) f(-k) - \sum_{k'} e^{ik'j} W(k=0) f(k')) \tag{3.40}$$

$$\implies = \frac{1}{L+1} (\sum_{k} e^{ikj} W(-k) f(k) - \sum_{k} e^{ikj} W(k=0) f(k)) \tag{3.41}$$

$$\implies = \frac{1}{L+1} \sum_{k} e^{ikj} (W(k) - W(k=0)) f(k) \tag{3.42}$$

We got the above by noting $W(k) = W(-k)$. Now, taking Fourier transform on both sides of Eq. 3.34, we get:

$$\partial_t f(k,t) = (W(k) - W(k=0)) f(k,t) \tag{3.43}$$

Now, using Eq. 3.35, we have:

$$W(k) - W(k=0) = \sum_{i-j=-L/2, i\neq j}^{L/2} (e^{-ik(i-j)} - 1) W_{i\to j} \tag{3.44}$$

$$\implies = \lambda \sum_{i-j=-L/2, i\neq j}^{L/2} \frac{e^{-ik(i-j)} - 1}{|i-j|^{2\alpha}} \tag{3.45}$$

$$\implies = 2\lambda \int_{1}^{L/2} dx\, (cos(kx) - 1)/x^{2\alpha} \tag{3.46}$$

$$\implies = 2\lambda \int_{0}^{L/2} dx\, (cos(kx) - 1)/x^{2\alpha} - 2\lambda \int_{0}^{1} dx\, (cos(kx) - 1)/x^{2\alpha} \tag{3.47}$$

For long times, large wavelengths dominate; therefore, we look at $k \ll 1$. For the second term, since x is upper bounded (by 1, which isn't extensive in system size), therefore, for $k \ll 1$, we have $kx \ll 1$, and we can do Taylor series expansion of the cosine about zero. Also, we can change the variables in the first term and take the upper bound to ∞

$$W(k) - W(k=0) = 2\lambda \int_0^\infty dx\,(cos(kx)-1)/x^{2\alpha} + \lambda k^2 \int_0^1 dx\, x^{2\alpha-1} \tag{3.48}$$

$$\implies = \lambda \left(-c_\alpha |k|^{2\alpha-1} + \frac{k^2}{3-2\alpha} \right) \tag{3.49}$$

Here,

$$c_\alpha = -2 \int_0^\infty dz \frac{cos(z)-1}{z^{2\alpha}} = -2\Gamma(1-2\alpha) sin(\alpha\pi) \tag{3.50}$$

Although going from Eq. 3.46 to Eq. 3.47 we assumed $\alpha < 1.5$, it is found that Eq. 3.49 is a valid approximation for the integral for all $\alpha > 0.5$. But it is expected to break down when α is large enough that approximating the sum as integral fails. We would later see that we require $\alpha > 1$ when we study the system size dependence of current.

Now, for $0.5 < \alpha < 1.5$, the term containing $|k|^{2\alpha-1}$ is leading, and hence from Eq. 3.43, we get

$$\partial_t f(k,t) = -\lambda c_\alpha |k|^{2\alpha-1} f(k,t) \implies f(k,t) = f(k,0) exp(-\lambda c_\alpha |k|^{2\alpha-1} t) \tag{3.51}$$

For initial localization, $f(k,0) = 1$, taking the fourier transform we arrive at:

$$f_j(t) \approx \int \frac{dk}{2\pi} exp(ikj - \lambda c_\alpha |k|^{2\alpha-1} t) = (D_\alpha t)^{-\beta_\alpha} F_\alpha \left(\frac{|j|}{(D_\alpha t)^{\beta_\alpha}} \right) \tag{3.52}$$

where, $\beta_\alpha = \frac{1}{2\alpha-1}$, $D_\alpha = \lambda c_\alpha$, and

$$F_\alpha(y) = \int \frac{dk}{2\pi} exp(-|k|^{1/\beta_\alpha}) exp(iyk) \tag{3.53}$$

For $\alpha > 1.5$, the second term is the leading term, and hence from Eq. 3.43, we get,

$$\partial_t f(k,t) = -\frac{\lambda}{2\alpha-3} k^2 f(k,t) \implies f(k,t) = f(k,0) exp(-\frac{\lambda}{2\alpha-3} k^2 t) \tag{3.54}$$

For initial localization, $f(k,0) = 1$, taking the fourier transform we arrive at:

$$f_j(t) \approx \int \frac{dk}{2\pi} exp(ikj - \frac{\lambda}{2\alpha - 3}k^2 t) = (D_\alpha t)^{-1/2} G\left(\frac{|j|}{(D_\alpha t)^{1/2}}\right) \tag{3.55}$$

where $D_\alpha = \frac{\lambda}{2\alpha-3}$, and $G(y) = \frac{exp(-y^2/4)}{2\sqrt{\pi}}$.

The scaling functions obtained here are exactly the ones that are used as analytic functions in Fig. 3.2 and Fig. 3.4. For $\alpha = 1.8$, because of finite times, even the first term in Eq. 3.49 has finite contributions leading to heavy tails deviating from the Gaussian scaling that is seen in the bulk. A modified analytical function, as derived in Ref. [21] is used in Fig. 3.3.

3.5 Connection with the Conductance exponent

Now, we have to get the system size scaling of the current that would flow through the open system. We know that for $0.5 < \alpha < 1.5$, we get a family of symmetric, $\alpha-$ dependent, stable distributions corresponding to classical Levy flights.

In accordance with Ref. [23], suppose in the probability distribution $P(x,t)$, $x \sim t^{1/\beta}$, then for an open system, current $J \sim L^{1-\beta}$, where L is the system size. We note that $\beta = 1/\beta_\alpha = 2\alpha - 1$. β is also known as the dynamical scaling exponent (z) characterizing the transport. For $\alpha > 1.5$, $\beta = 2$, i.e., the dynamics is diffusive. Therefore, we get:

$$J \sim L^{2-2\alpha} \qquad \text{for } 1 < \alpha < 1.5 \tag{3.56}$$

$$J \sim L^{-1} \qquad \text{for } \alpha > 1.5 \tag{3.57}$$

This exactly matches the scaling of conductance we got in the previous chapter. There is a slight subtlety that remains. In Ref. [23], the classical master equation is slightly different, leading to ballistic peaks at the extreme ends of the dynamic probability distribution. But, the conductance

exponent remains the same, as verified numerically in [24]. This completes the analytical calculations that is consistent with the numerical results.

Chapter 4

Quantum Transport in Quasi 1D Lattice Systems

In this chapter, we shift our focus to different ladder setups which are quasi one-dimensional lattice systems. We study fermionic transport in such open ladder setups. It is important to study because they form the connecting link between 1D and 2D systems. Ladders with quasiperiodic potential have been used to model molecular structures like artificial DNA, which can be used for rectification purposes [25]. Spin ladders are also interesting owing to their relation with high-temperature superconductivity [26]. We first start with finding transfer matrices and their exceptional points (EPs) for various ladder models. Then, a general relation is provided between transfer matrices and band spectra of the model. Furthermore, the conductance is expressed in terms of transfer matrix elements, which provides a useful way to extract the scaling of conductance analytically. The phase diagram for a ladder with a gauge field [27] is looked at with the lens of steady-state quantum transport. We end the chapter by providing some interesting transport properties dependent on the geometry of the baths' placement and the system size's parity.

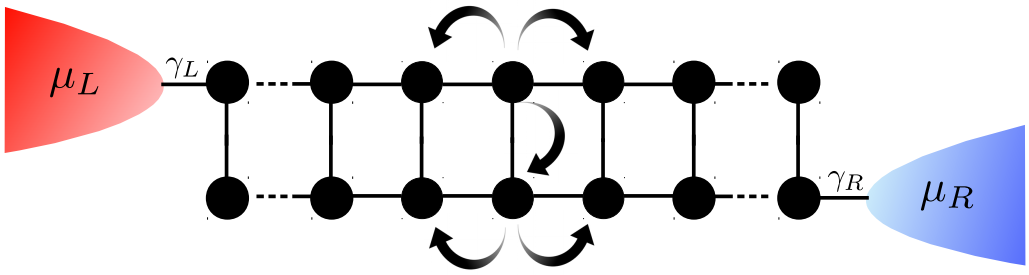

Figure 4.1: A schematic of a simple ladder set-up driven by boundary baths. The baths could be placed in either of the legs, and the figure shows one possibility.

4.1 Transfer Matrix analysis for different ladder models

4.1.1 Simple ladder with nearest neighbor hopping

The Hamiltonian is given by:

$$H_S = -t_1 \sum_{j=1}^{N-1} (c_{1,j}^\dagger c_{1,j+1} + h.c.) - t_2 \sum_{j=1}^{N-1} (c_{2,j}^\dagger c_{2,j+1} + h.c.) - t_r \sum_{j=1}^{N} (c_{1,j}^\dagger c_{2,j} + h.c.) \tag{4.1}$$

Now, let's formulate the transfer matrix for our model. Let $\begin{pmatrix} \psi_1 & \psi_2 & \cdots \psi_N \end{pmatrix}^T$ denote the energy eigenfunction vector (with the element ψ_i denoting the energy eigenfunction amplitude at the site i for the top leg). Similarly, let $\begin{pmatrix} \phi_1 & \phi_2 & \cdots \phi_N \end{pmatrix}^T$ denote the energy eigenfunction vector for the bottom leg of the ladder. Let the corresponding energy be ε. Then, from the time-independent Schrodinger equation, we have:

$$\varepsilon \psi_n = -t_1 \psi_{n+1} - t_1 \psi_{n-1} - t_r \phi_n \tag{4.2}$$

$$\varepsilon \phi_n = -t_2 \phi_{n+1} - t_2 \phi_{n-1} - t_r \psi_n \tag{4.3}$$

$$\implies \psi_{n+1} = -\frac{\varepsilon}{t_1} \psi_n - \psi_{n-1} - \frac{t_r}{t_1} \phi_n \tag{4.4}$$

$$\phi_{n+1} = -\frac{\varepsilon}{t_2} \phi_n - \phi_{n-1} - \frac{t_r}{t_2} \psi_n \tag{4.5}$$

The above equations can be written in terms of the transfer matrix as follows:

$$\begin{pmatrix} -\frac{\varepsilon}{t_1} & -\frac{t_r}{t_1} & -1 & 0 \\ -\frac{t_r}{t_2} & -\frac{\varepsilon}{t_2} & 0 & -1 \\ 1 & 0 & 0 & 0 \\ 0 & 1 & 0 & 0 \end{pmatrix} \begin{pmatrix} \psi_n \\ \phi_n \\ \psi_{n-1} \\ \phi_{n-1} \end{pmatrix} = \begin{pmatrix} \psi_{n+1} \\ \phi_{n+1} \\ \psi_n \\ \phi_n \end{pmatrix} \tag{4.6}$$

It can be verified that Det(T) is 1, where T is the above transfer matrix.

Symmetric hopping simple ladder

Let us analyze the above transfer matrix for the case of $t_1 = t_2 = t$. Let $a = -\frac{\varepsilon}{t}$ and $b = -\frac{t_r}{t}$, for simplicity. Therefore, the transfer matrix now becomes:

$$T = \begin{pmatrix} a & b & -1 & 0 \\ b & a & 0 & -1 \\ 1 & 0 & 0 & 0 \\ 0 & 1 & 0 & 0 \end{pmatrix} \tag{4.7}$$

Then, it can be diagonalized and written as $T = SJS^{-1}$ where

$$\mathrm{S} = \begin{pmatrix} \frac{1}{2}\left(\sqrt{(a-b)^2-4}-a+b\right) & \frac{1}{2}\left(-\sqrt{(a-b)^2-4}-a+b\right) & \frac{1}{2}\left(-\sqrt{(a+b)^2-4}+a+b\right) & \frac{1}{2}\left(\sqrt{(a+b)^2-4}+a+b\right) \\ \frac{1}{2}\left(-\sqrt{(a-b)^2-4}+a-b\right) & \frac{1}{2}\left(\sqrt{(a-b)^2-4}+a-b\right) & \frac{1}{2}\left(-\sqrt{(a+b)^2-4}+a+b\right) & \frac{1}{2}\left(\sqrt{(a+b)^2-4}+a+b\right) \\ -1 & -1 & 1 & 1 \\ 1 & 1 & 1 & 1 \end{pmatrix}$$

$$\mathrm{J} = \begin{pmatrix} \frac{1}{2}\left(-\sqrt{(a-b)^2-4}+a-b\right) & 0 & 0 & 0 \\ 0 & \frac{1}{2}\left(\sqrt{(a-b)^2-4}+a-b\right) & 0 & 0 \\ 0 & 0 & \frac{1}{2}\left(-\sqrt{(a+b)^2-4}+a+b\right) & 0 \\ 0 & 0 & 0 & \frac{1}{2}\left(\sqrt{(a+b)^2-4}+a+b\right) \end{pmatrix}$$

Now, the columns of matrix S represent the right eigenvectors (the left eigenvectors of T will be the rows of S^{-1}). Clearly, it is not possible to have a fourth-order exceptional point. The first

two eigenvectors merge when $a-b=\pm 2$, while the last two eigenvectors merge when $a+b=\pm 2$. Therefore, there can be at most two second-order exceptional points, given an energy.

By substituting the values of a and b, we find that all the exceptional points occur at band edges ($k=0,\pm\pi$).

Two second-order exceptional points occur for two cases:

- $a=\pm 2$, $b=0$. This case is when the two bands merge into one single band. But in this case, since $t_r=0$, it means that the two legs of the ladder are disconnected; hence, the system should be describable using two transfer matrices, one for each leg. This would yield a second-order exceptional point at the band edges for each transfer matrix. Therefore, we are in fact getting two second-order exceptional points for our 4×4 transfer matrix.

- $a=0$, $b=\pm 2$. This case is more interesting. It lies at the boundary of gapped and ungapped regions. Notice that at $\varepsilon=0$, we find two degenerate states, corresponding to $k=0$ and $k=\pi(\text{or } -\pi)$.

Asymmetric hopping simple ladder

We now consider the general case of asymmetric hopping in the two legs. Using the band dispersion, we will get the exceptional points of the general transfer matrix for this model. This already indicates a deeper relation between them, which is proved later.

We diagonalize the Hamiltonian exploiting translational invariance of the Hamiltonian (in thermodynamic limit or by imposing periodic boundary conditions) and get the energy dispersion relation as follows:

$$m=E_k^{\pm}=-(t_1+t_2)\cos(k)\pm\sqrt{(t_1-t_2)^2\cos^2(k)+t_r^2} \tag{4.8}$$

When $t_1 = t_2 = t$, the energy spectrum reduces to:

$$E_k^{\pm} = -2t\cos(k) \pm t_r \tag{4.9}$$

Exceptional Points for the asymmetric hopping in the ladder by analyzing the band

It is observed that the odd derivatives of the dispersion relation vanish at $k = 0, \pi$ because of the parity of the function.

Therefore, a second-order exceptional point always exists for $k = 0, \pi$. Now, we want to look for the fourth-order exceptional point, which is the highest that we can get given the dimension of the transfer matrix. For that we need the second derivative also to vanish. Since the third derivative must vanish, we'd get a fourth-order exceptional point when the second derivative vanishes.

Let $t_1 + t_2 = a$, $t_1 - t_2 = b$ and $t_r = c$, for the ease of writing. The second derivative is found to be:

$$\frac{\mathrm{d}^2 E_k^{\pm}}{\mathrm{d}k^2} = a\cos(k) \pm \left(-\frac{b^2\cos^2(k)}{\sqrt{b^2\cos^2(k) + c^2}} + \frac{b^2\sin^2(k)}{\sqrt{b^2\cos^2(k) + c^2}} - \frac{b^4\sin^2(k)\cos^2(k)}{(b^2\cos^2(k) + c^2)^{3/2}} \right) \tag{4.10}$$

At $k = 0, \pi$, we have it simplified to:

$$\frac{\mathrm{d}^2 E_k^{\pm}}{\mathrm{d}k^2} = a\cos(k) \pm \frac{-b^2}{\sqrt{b^2 + c^2}} \tag{4.11}$$

Setting the second derivative to zero, we observe that we get fourth-order exceptional points at $k = 0$ for the upper band and $k = \pi$ for the lower band when:

$$a = \frac{b^2}{\sqrt{b^2 + c^2}} \tag{4.12}$$

And we get the opposite, i.e fourth order exceptional points at $k = 0$ for the lower band and $k = \pi$

for the upper band when:

$$a = -\frac{b^2}{\sqrt{b^2+c^2}} \tag{4.13}$$

Now, $t_1 = (a+b)/2$ and $t_2 = (a-b)/2$. The above equations will help us find the exact hopping amplitudes for both legs to get exceptional fourth-order points.

4.1.2 Crossed ladder

Consider the following setup. We will write the transfer matrix for this. Let the hopping amplitude

Figure 4.2: Crossed Ladder

along the legs be t, along the rungs be t_r, and along the crosses be t_s. Then, using the time-independent Schrodinger equation, we have:

$$\varepsilon\psi_n = -t\psi_{n+1} - t\psi_{n-1} - t_r\phi_n - t_s\phi_{n+1} - t_s\phi_{n-1} \tag{4.14}$$

$$\varepsilon\phi_n = -t\phi_{n+1} - t\phi_{n-1} - t_r\psi_n - t_s\psi_{n+1} - t_s\psi_{n-1} \tag{4.15}$$

$$\implies \psi_{n+1} = -\frac{\varepsilon}{t}\psi_n - \psi_{n-1} - \frac{t_r}{t}\phi_n - \frac{t_s}{t}\phi_{n+1} - \frac{t_s}{t}\phi_{n-1} \tag{4.16}$$

$$\phi_{n+1} = -\frac{\varepsilon}{t}\phi_n - \phi_{n-1} - \frac{t_r}{t}\psi_n - \frac{t_s}{t}\psi_{n+1} - \frac{t_s}{t}\psi_{n-1} \tag{4.17}$$

We'll use the equation for ϕ_{n+1} to get:

$$t_s t\psi_{n+1} = -\varepsilon t\phi_n - t^2\phi_{n-1} - t^2\phi_{n+1} - t_r t\psi_n - t_s t\psi_{n-1} \tag{4.18}$$

But we also have:

$$\psi_{n+1} = -\frac{\varepsilon}{t}\psi_n - \psi_{n-1} - \frac{t_r}{t}\phi_n - \frac{t_s}{t}\phi_{n+1} - \frac{t_s}{t}\phi_{n-1} \tag{4.19}$$

$$\implies t_s t\,\psi_{n+1} = -t_s\varepsilon\,\psi_n - t_s t\,\psi_{n-1} - t_r t_s\phi_n - {t_s}^2\phi_{n+1} - {t_s}^2\phi_{n-1} \tag{4.20}$$

Comparing the equations for $t_s t\,\psi_{n+1}$, we have:

$$-\varepsilon t\,\phi_n - t^2\phi_{n-1} - t^2\phi_{n+1} - t_r t\,\psi_n - t_s t\,\psi_{n-1} = -t_s\varepsilon\,\psi_n - t_s t\,\psi_{n-1} - t_r t_s\phi_n - {t_s}^2\phi_{n+1} - {t_s}^2\phi_{n-1} \tag{4.21}$$

We finally get:

$$(t_s^2 - t^2)\phi_{n+1} = (\varepsilon t - t_r t_s)\phi_n + (t^2 - t_s^2)\phi_{n-1} + (t_r t - t_s\varepsilon)\psi_n \tag{4.22}$$

Similarly, we get:

$$(t_s^2 - t^2)\psi_{n+1} = (\varepsilon t - t_r t_s)\psi_n + (t^2 - t_s^2)\psi_{n-1} + (t_r t - t_s\varepsilon)\phi_n \tag{4.23}$$

Therefore, we see that we get a 4×4 transfer matrix for the crossed ladder. Also, note that for $t_s = \pm t$, we note that the recursion relation ceases to exist.

$$T = \begin{pmatrix} \frac{\varepsilon t - t_r t_s}{t_s^2 - t^2} & \frac{t_r t - t_s\varepsilon}{t_s^2 - t^2} & -1 & 0 \\ \frac{t_r t - t_s\varepsilon}{t_s^2 - t^2} & \frac{\varepsilon t - t_r t_s}{t_s^2 - t^2} & 0 & -1 \\ 1 & 0 & 0 & 0 \\ 0 & 1 & 0 & 0 \end{pmatrix} = \begin{pmatrix} a' & b' & -1 & 0 \\ b' & a' & 0 & -1 \\ 1 & 0 & 0 & 0 \\ 0 & 1 & 0 & 0 \end{pmatrix} \tag{4.24}$$

By inspecting the structure of the transfer matrix, which is similar to the symmetric hopping case with a simple ladder, we can conclude that there is no fourth-order exceptional point for this matrix.

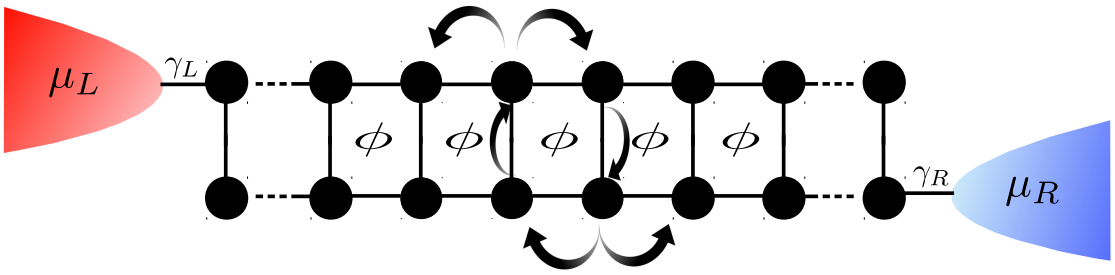

Figure 4.3: A schematic of a simple ladder in the presence of a gauge field, driven by boundary baths. The boundary baths could have also been on the same leg.

4.1.3 Simple ladder with gauge field

Here, we study a simple fermionic ladder with a perpendicular gauge field. The Hamiltonian for the system is given by:

$$H_S = -\left(J^{\parallel} \sum_{l,p} e^{i\frac{\phi}{2}(-1)^{p+1}} a^{\dagger}_{l,p} a_{l+1,p} + J^{\perp} \sum_{l} a^{\dagger}_{l,1} a_{l,2} + h.c. \right) \tag{4.25}$$

The dispersion relation yields two bands obtained using the Bogoliubov transformation [27] and is given by:

$$\varepsilon_k^{\pm} = -2J^{\parallel} \cos(\phi/2) \cos(k) \pm \sqrt{J^{\perp 2} + (2J^{\parallel} \sin(\phi/2) \sin(k))^2} \tag{4.26}$$

Here, the k does not denote the momentum label of the particle. It is rather denoting quasiparticle momenta.

As before, let $|\psi\rangle$ and $|\phi\rangle$ be energy eigenvectors for the top and bottom leg of the ladder (i.e p=1 and 2, respectively) with $|\psi\rangle = \begin{pmatrix} \psi_1 & \psi_2 & \cdots \psi_N \end{pmatrix}^T$ and $|\phi\rangle = \begin{pmatrix} \phi_1 & \phi_2 & \cdots \phi_N \end{pmatrix}^T$, both

written in the position basis, as before. Now, using Schrodinger equation gives us:

$$\varepsilon\psi_n = -J^{\parallel}e^{i\phi/2}\psi_{n+1} - J^{\parallel}e^{-i\phi/2}\psi_{n-1} + J^{\perp}\phi_n \tag{4.27}$$

$$\varepsilon\phi_n = -J^{\parallel}e^{-i\phi/2}\phi_{n+1} - J^{\parallel}e^{i\phi/2}\phi_{n-1} + J^{\perp}\psi_n \tag{4.28}$$

$$\implies \psi_{n+1} = -\frac{\varepsilon}{J^{\parallel}}e^{-i\phi/2}\psi_n - e^{-i\phi}\psi_{n-1} - \frac{J^{\perp}}{J^{\parallel}}e^{-i\phi/2}\phi_n \tag{4.29}$$

$$\phi_{n+1} = -\frac{\varepsilon}{J^{\parallel}}e^{i\phi/2}\phi_n - e^{i\phi}\phi_{n-1} - \frac{J^{\perp}}{J^{\parallel}}e^{i\phi/2}\psi_n \tag{4.30}$$

In terms of the transfer matrix we have:-

$$\begin{pmatrix} -\frac{\varepsilon}{J^{\parallel}}e^{-i\phi/2} & -\frac{J^{\perp}}{J^{\parallel}}e^{-i\phi/2} & -e^{-i\phi} & 0 \\ -\frac{J^{\perp}}{J^{\parallel}}e^{i\phi/2} & -\frac{\varepsilon}{J^{\parallel}}e^{i\phi/2} & 0 & -e^{i\phi} \\ 1 & 0 & 0 & 0 \\ 0 & 1 & 0 & 0 \end{pmatrix} \begin{pmatrix} \psi_n \\ \phi_n \\ \psi_{n-1} \\ \phi_{n-1} \end{pmatrix} = \begin{pmatrix} \psi_{n+1} \\ \phi_{n+1} \\ \psi_n \\ \phi_n \end{pmatrix} \tag{4.31}$$

Now, the opening of the band gap is given by the condition:

$$J_c^{\perp} = 2J^{\parallel}\cos(\phi/2) \tag{4.32}$$

The Meissner to Vortex quantum phase transition is observed in a fermionic system where an artificial gauge field is generated using superconducting qubit circuits [28]. The ground state properties change across the transition, which is given by:

$$J_c^{\perp} = 2J^{\parallel}\tan(\phi/2)\sin(\phi/2) \tag{4.33}$$

Before proceeding, we'll briefly derive the equations of the special lines.

The Meissner-Vortex Line: We note that the line is characterized by the vanishing of the second derivative of the band (upper or lower at $k = 0, \pi$ depending on the parameters, as we shall see).

$$\frac{\mathrm{d}^2\varepsilon_k^{\pm}}{\mathrm{d}k^2} = 2J^{\parallel}\cos(\phi/2)\cos(k) \pm \left(\frac{(2J^{\parallel}\sin(\phi/2))^2\cos(2k)}{\sqrt{J^{\perp 2} + (2J^{\parallel}\sin(\phi/2)\sin(k))^2}} - \frac{4(J^{\parallel}\sin(\phi/2))^2\sin(2k)^2}{(J^{\perp 2} + (2J^{\parallel}\sin(\phi/2)\sin(k))^2)^{3/2}} \right) \tag{4.34}$$

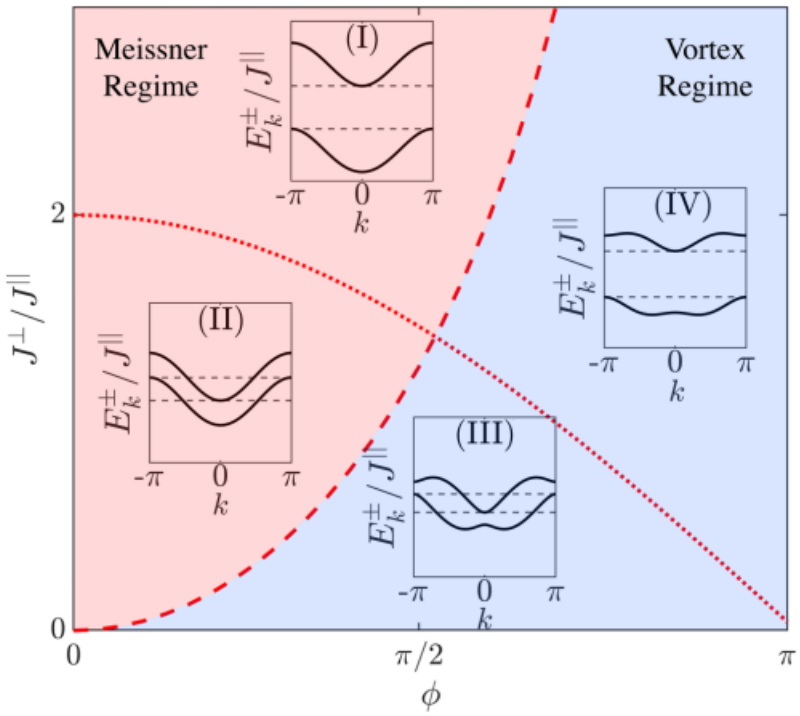

Figure 4.4: Band structures and phase diagram for a ladder in a gauge field. Figure included from [27].

Now, let us take $k = 0$ and set the second derivative to zero:

$$\frac{\mathrm{d}^2\varepsilon_k^{\pm}}{\mathrm{d}k^2} = 2J^{\parallel}\cos(\phi/2) \pm \frac{(2J^{\parallel}\sin(\phi/2))^2}{|J^{\perp}|} = 0 \tag{4.35}$$

$$\implies |J^{\perp}| = \mp 2J^{\parallel}\tan(\phi/2)\sin(\phi/2) \tag{4.36}$$

Therefore, to have a fourth-order exceptional point for the upper band at $k = 0$, we must have $J^{\parallel}$ to be negative. The dispersion relation is insensitive to the sign of $J^{\perp}$.

Now, the same procedure can be done for $k = \pi$. Interestingly, it is found that both the points (i.e., for $k = 0, \pi$) develop fourth-order EPs simultaneously, one for the upper band and the other for the lower band, with the exact locations determined by the sign of $J^{\parallel}$ (and also the quadrant to which ϕ belongs if its range is extended). When $J^{\parallel}$ is positive, and $\phi \in [-\pi, \pi]$, then the fourth order EP occurs at $k = \pi$ for the upper band and $k = 0$ for the lower band, while when $J^{\parallel}$ is neg-

ative, and $\phi \in [-\pi, \pi]$, then the fourth order EP occurs at $k = \pi$ for the lower band and $k = 0$ for the upper band.

The Gapped-ungapped line: This line marks the transition from gapped to ungapped phases. Therefore, the line is characterized by the energy corresponding to the global minima of the upper band, which should match the energy corresponding to the global maxima of the upper band.

It can be easily verified that the required extremum either corresponds to $k = 0$ or $k = \pi$ depending on the parameters.

$$\varepsilon^{\pm}_{k=0} = -2J^{\parallel}\cos(\phi/2) \pm \left|J^{\perp}\right| \tag{4.37}$$

$$\varepsilon^{\pm}_{k=\pi} = 2J^{\parallel}\cos(\phi/2) \pm \left|J^{\perp}\right| \tag{4.38}$$

Now, $\varepsilon^{+}_{k=0} = \varepsilon^{-}_{k=\pi}$ yields:-

$$\left|J^{\perp}\right| = 2J^{\parallel}\cos(\phi/2) \tag{4.39}$$

And, having $\varepsilon^{-}_{k=0} = \varepsilon^{+}_{k=\pi}$ yields:-

$$\left|J^{\perp}\right| = -2J^{\parallel}\cos(\phi/2) \tag{4.40}$$

The above completes the derivation for the two special lines in the phase diagram in Fig. 4.4. Also, it extends the phase diagram by including the negative hopping amplitudes.

The characteristic equation for the gauge field ladder

Let's rewrite the general transfer matrix for the ladder with gauge field ϕ by substituting $-\frac{\varepsilon}{J^{\parallel}} = a$ and $-\frac{J^{\perp}}{J^{\parallel}} = b$

$$\begin{pmatrix} ae^{-i\phi/2} & be^{-i\phi/2} & -e^{-i\phi} & 0 \\ be^{i\phi/2} & ae^{i\phi/2} & 0 & -e^{i\phi} \\ 1 & 0 & 0 & 0 \\ 0 & 1 & 0 & 0 \end{pmatrix} \tag{4.41}$$

The characteristic equation for eigenvalue x is given by:

$$x^4 - 2ax^3\cos\left(\frac{\phi}{2}\right) + \left(a^2 - b^2 + 2\cos(\phi)\right)x^2 - 2ax\cos\left(\frac{\phi}{2}\right) + 1 = 0 \tag{4.42}$$

The above can provide the eigenvalues and their multiplicities for various parameter values. After that, to check for an exceptional point, the merging of eigenvectors needs to be ascertained.

On the Meissner-Vortex line

It is found that up to three derivatives of the band spectra vanish for $k = \pm\pi$ for the upper band and $k = 0$ for the lower band.

This is intuitively expected because the band changes its extrema properties at these points. More clearly, take, for instance, the upper band. In the Meissner regime, there is a maximum at $k = \pi$. Now, this changes to a local minimum as the line is crossed. For this to happen, the second derivative must vanish at the line. It turns out that the third derivative also vanishes. This indicates the presence of a fourth-order exceptional point on the line.

This is more clearly seen by explicitly calculating the eigenvalues using the general characteristic equation. For the Meissner-Vortex line, we have:

- For the upper band at $k = \pi$:

$$\begin{aligned} b &= -2\tan(\phi/2)\sin(\phi/2) \\ a &= -\frac{(2J^{\parallel}\cos(\phi/2) + J^{\perp})}{J^{\parallel}} \implies a = -\frac{2}{\cos(\phi/2)} \end{aligned}$$

Substituting this in the characteristic equation, we get the characteristic equation to be:

$$\begin{aligned} & x^4 + 4x^3 + 6x^2 + 4x + 1 = 0 \\ \implies & (x+1)^4 = 0 \end{aligned}$$

Therefore, there is an eigenvalue -1 of the transfer matrix for the upper band at $k = \pi$, with multiplicity 4. The four eigenvectors of the transfer matrix also coalesce, making it a fourth-order exceptional point.

- For the lower band at $k = 0$:

$$\begin{aligned} b &= -2\tan(\phi/2)\sin(\phi/2) \\ a &= \frac{2}{\cos(\phi/2)} \end{aligned}$$

The characteristic equation then comes out to be:

$$\begin{aligned} & x^4 - 4x^3 + 6x^2 - 4x + 1 = 0 \\ \implies & (x-1)^4 = 0 \end{aligned}$$

This implies a fourth-order exceptional point at $k = 0$, with eigenvalue 1.

On the gapped-ungapped line

This line hosts two second-order exceptional points with real eigenvalues 1 and -1 corresponding to points $k = 0$ and π, respectively, at the energy value 0. This happens because, at this energy, we have a minimum for the upper band (at $k = 0$) and a maximum for the lower band at $k = \pi$.

Now, we will explicitly solve the characteristic equation for the transfer matrix at zero energy for this gapped-ungapped line.

$$b = -2\cos(\phi/2)$$
$$a = 0$$

Therefore, the characteristic equation becomes:

$$x^4 - 2x^2 + 1 = 0$$
$$\implies x = \pm 1$$

The multiplicity is 2 for both the eigenvalues. Since the eigenvectors also merge, this implies two second-order exceptional points, one at $k = 0$ and the other at $k = \pi$.

4.2 General Relation between the Transfer Matrix and the Band spectrum

4.2.1 Discrete Translational Symmetry

The discrete translational symmetry is essential for having a transfer matrix formulation of the problem. Now, I will use this symmetry to see how the transfer matrix can be used to get the energy dispersion relation in general.

We have assumed a unit distance separating the lattice points. Let the unit cell be of length b, i.e., a translation by b units will leave the system unchanged. Let T_{nb} be the translation operator, translating by nb units, where n is an integer. Then $[T_{nb}, H] = 0$. Therefore, it is possible to find an energy basis comprising of eigenstates of T_b. Let $|\psi\rangle$ be such a state. Now, note that T_b is a unitary operator. Therefore, we have:

$$T_b |\psi\rangle = e^{ikb} |\psi\rangle \tag{4.43}$$

Note that b got factored out in the phase. This is because we also need to satisfy the following property of translation operators: $T_{nb}T_{mb} = T_{(n+m)b}$. Note that k is the momentum (and sometimes quasimomentum) that labels the energies. k is unique only in some range, and we conveniently chose it to be the Brillouin zone. Also, when k is restricted to be in the Brillouin zone, every energy eigenstate has a single k value associated with it, but the converse doesn't hold, as we can have multiple bands.

As we shall see in the next section, Eq. 4.43 is essential to establish a connection between transfer matrix eigenvalues and the band spectra.

4.2.2 The General Relation

In this section, I will state and prove the relation for a one-dimensional chain, but it is easily extended for the case of ladders.

Let M be the transfer matrix for a one-dimensional system (at some particular energy) with nearest neighbor hopping. Then, for any n, we will have:

$$M \begin{pmatrix} \psi_n \\ \psi_{n-1} \end{pmatrix} = \begin{pmatrix} \psi_{n+1} \\ \psi_n \end{pmatrix} \tag{4.44}$$

Now, because the system has translational invariance, using Eq. 4.43 we have:

$$M \begin{pmatrix} \psi_n \\ \psi_{n-1} \end{pmatrix} = \begin{pmatrix} \psi_{n+1} \\ \psi_n \end{pmatrix} = \begin{pmatrix} e^{ik}\psi_n \\ e^{ik}\psi_{n-1} \end{pmatrix} = e^{ik} \begin{pmatrix} \psi_n \\ \psi_{n-1} \end{pmatrix} \tag{4.45}$$

The above implies that the eigenvector(s) and eigenvalue(s) of M are given by $\begin{pmatrix} \psi_n \\ \psi_{n-1} \end{pmatrix}$ and e^{ik}. Since M depends on the energy, this gives a relation us the band dispersion starting from the

transfer matrix.

Note that for the energies not in the system's spectrum, the transfer matrix's eigenvalue won't be a unit complex number as required otherwise.

4.3 Greens's function and the transfer matrix for the ladder

4.3.1 Asymmetric hopping ladder

To calculate the conductance, we need to know the Non-equilibrium Green's function (NEGF). It is given by:

$$G(\mu) = (\mu\mathbb{1} - H - \Sigma_s - \Sigma_d)^{-1} \tag{4.46}$$

Since we only need to know the scaling of conductance, we can use the bare Green's function of the system without the self-energy terms. Therefore, we have:

$$G_0(\mu) = (\mu\mathbb{1} - H)^{-1} \tag{4.47}$$

Now, the translation symmetry and the banded nature of $\mu\mathbb{1} - H$, will help us to calculate the inverse using the transfer matrix powers. The following procedure is a generalization of the calculation in [29], and follows analogously. Let $M(\mu) = \mu\mathbb{1} - H$. Therefore, we need to find $M(\mu)^{-1}$. By definition, we have:

$$\sum_j \langle i|M(\mu)|j\rangle \, \langle j|M(\mu)^{-1}|k\rangle = \delta_{ik} \tag{4.48}$$

Let, $m = j - i$

$$\sum_{m=\alpha(i)}^{\beta(i)} \langle i|M(\mu)|i+m\rangle \, \langle i+m|M(\mu)^{-1}|k\rangle = \delta_{ik} \tag{4.49}$$

From now on, for simplicity of notation, I'll write $M(\mu) \equiv M$. For any odd $i > 1$, we get the following.

$$t_1 \langle i-2|M^{-1}|k\rangle + \mu \langle i|M^{-1}|k\rangle + t_r \langle i+1|M^{-1}|k\rangle + t_1 \langle i+2|M^{-1}|k\rangle = \delta_{ik} \tag{4.50}$$

Similarly, for any even $i > 2$, we will get:

$$t_2 \langle i-2|M^{-1}|k\rangle + t_r \langle i-1|M^{-1}|k\rangle + \mu \langle i|M^{-1}|k\rangle + t_2 \langle i+2|M^{-1}|k\rangle = \delta_{ik} \tag{4.51}$$

Now, it can be verified that we get exactly the above two relations from the transfer matrix in the following manner:

$$\begin{pmatrix} -\frac{\mu}{t_1} & -\frac{t_r}{t_1} & -1 & 0 \\ -\frac{t_r}{t_2} & -\frac{\mu}{t_2} & 0 & -1 \\ 1 & 0 & 0 & 0 \\ 0 & 1 & 0 & 0 \end{pmatrix} \begin{pmatrix} \langle i|M^{-1}|k\rangle \\ \langle i+1|M^{-1}|k\rangle \\ \langle i+2|M^{-1}|k\rangle \\ \langle i+3|M^{-1}|k\rangle \end{pmatrix} = \begin{pmatrix} \langle i-2|M^{-1}|k\rangle - \frac{\delta_{ik}}{t_1} \\ \langle i-1|M^{-1}|k\rangle - \frac{\delta_{ik}}{t_2} \\ \langle i|M^{-1}|k\rangle \\ \langle i+1|M^{-1}|k\rangle \end{pmatrix} \tag{4.52}$$

In the above equation, i is odd. This implies $i+1$ is even, and this satisfies the even row index equation. If i is chosen, even then, we will have to take slightly different vectors.

To be clear, the sites are labeled such that all the odd indices label the sites in the upper leg, and the even indices label the sites in the lower leg.

The above relation strongly motivates us to define a starting vector to construct the matrix elements of M^{-1}. For notation purposes, changing the dummy index k to j. Let the vector be:

$$V_{-1}(j) = \begin{pmatrix} 0 \\ 0 \\ \langle 1|M^{-1}|j\rangle \\ \langle 2|M^{-1}|j\rangle \end{pmatrix} \tag{4.53}$$

For notational ease, we assume that $\langle i|M^{-1}|j\rangle$ is 0 if the indices go out of bound. Then define,

$$V_i(j) = \begin{pmatrix} \langle i|M^{-1}|j\rangle \\ \langle i+1|M^{-1}|j\rangle \\ \langle i+2|M^{-1}|j\rangle \\ \langle i+3|M^{-1}|j\rangle \end{pmatrix}; \qquad |\mathbf{1}\rangle = \begin{pmatrix} 1 \\ 0 \\ 0 \\ 0 \end{pmatrix}; \qquad |\mathbf{2}\rangle = \begin{pmatrix} 0 \\ 1 \\ 0 \\ 0 \end{pmatrix} \tag{4.54}$$

Note that we are always taking i to be odd. Then, we can write:

$$T(\mu)V_i(j) = V_{i-2}(j) - \frac{\delta_{i,j}\,|\mathbf{1}\rangle}{t_1} - \frac{\delta_{i+1,j}\,|\mathbf{2}\rangle}{t_2} \tag{4.55}$$

Finally, we obtain:

$$V_i(j) = T(\mu)^{-\frac{i+1}{2}} V_{-1}(j), \qquad \text{if } j > i+1 \tag{4.56}$$

$$V_i(j) = T(\mu)^{-\frac{i+1}{2}} V_{-1}(j) - T(\mu)^{-(\frac{i-j}{2}+1)} \frac{|\mathbf{1}\rangle}{t_1}, \qquad \text{if } j < i+1 \text{ and odd} \tag{4.57}$$

$$V_i(j) = T(\mu)^{-\frac{i+1}{2}} V_{-1}(j) - T(\mu)^{-(\frac{i-j+1}{2}+1)} \frac{|\mathbf{2}\rangle}{t_2}, \qquad \text{if } j \leq i+1 \text{ and even} \tag{4.58}$$

Now, $V_i(j)$ contains the matrix elements of M^{-1}. We finally get:

$$\langle i|M^{-1}|j\rangle = \sum_{m=1}^{2} \langle 1|T(\mu)^{-\frac{i+1}{2}}|2+m\rangle \langle m|M^{-1}|j\rangle, \qquad \text{if } j > i+1 \tag{4.59}$$

$$\langle i|M^{-1}|j\rangle = \sum_{m=1}^{2} \langle 1|T(\mu)^{-\frac{i+1}{2}}|2+m\rangle \langle m|M^{-1}|j\rangle - \frac{\langle 1|T(\mu)^{-(\frac{i-j}{2}+1)}|1\rangle}{t_1}, \qquad \text{if } j < i+1 \text{ \& odd} \tag{4.60}$$

$$\langle i|M^{-1}|j\rangle = \sum_{m=1}^{2} \langle 1|T(\mu)^{-\frac{i+1}{2}}|2+m\rangle \langle m|M^{-1}|j\rangle - \frac{\langle 1|T(\mu)^{-(\frac{i-j+1}{2}+1)}|2\rangle}{t_2}, \qquad \text{if } j \leq i+1 \text{ \& even} \tag{4.61}$$

$$\langle i+1|M^{-1}|j\rangle = \sum_{m=1}^{2} \langle 2|T(\mu)^{-\frac{i+1}{2}}|2+m\rangle \langle m|M^{-1}|j\rangle, \qquad \text{if } j > i+1 \tag{4.62}$$

$$\langle i+1|M^{-1}|j\rangle = \sum_{m=1}^{2} \langle 2|T(\mu)^{-\frac{i+1}{2}}|2+m\rangle \langle m|M^{-1}|j\rangle - \frac{\langle 2|T(\mu)^{-(\frac{i-j}{2}+1)}|1\rangle}{t_1}, \qquad \text{if } j < i+1 \text{ \& odd} \tag{4.63}$$

$$\langle i+1|M^{-1}|j\rangle = \sum_{m=1}^{2} \langle 2|T(\mu)^{-\frac{i+1}{2}}|2+m\rangle \langle m|M^{-1}|j\rangle - \frac{\langle 2|T(\mu)^{-(\frac{i-j+1}{2}+1)}|2\rangle}{t_2}, \qquad \text{if } j \leq i+1 \text{ \& even} \tag{4.64}$$

Now, if we can find $\langle m|M^{-1}|j\rangle$ for $m = 1,2$, then we have all the matrix elements of the bare Green's function. This is achieved by noting that the last two entries of $V_{2N-1}(j)$ are 0. There are two subcases: j is odd or even. For each of these cases, we get two linear equations in two variables, which can be solved for $\langle m|M^{-1}|j\rangle$. When j is odd, we have:

$$\sum_{m=1}^{2} \langle 3|T(\mu)^{-N}|2+m\rangle \langle m|M^{-1}|j\rangle - \frac{\langle 3|T(\mu)^{-(\frac{2N+1-j}{2})}|1\rangle}{t_1} = 0 \tag{4.65}$$

$$\sum_{m=1}^{2} \langle 4|T(\mu)^{-N}|2+m\rangle \langle m|M^{-1}|j\rangle - \frac{\langle 4|T(\mu)^{-(\frac{2N+1-j}{2})}|1\rangle}{t_1} = 0 \tag{4.66}$$

When j is even, we have:

$$\sum_{m=1}^{2} \langle 3|T(\mu)^{-N}|2+m\rangle \langle m|M^{-1}|j\rangle - \frac{\langle 3|T(\mu)^{-(N+1-\frac{j}{2})}|2\rangle}{t_2} = 0 \tag{4.67}$$

$$\sum_{m=1}^{2} \langle 4|T(\mu)^{-N}|2+m\rangle \langle m|M^{-1}|j\rangle - \frac{\langle 4|T(\mu)^{-(N+1-\frac{j}{2})}|2\rangle}{t_2} = 0 \tag{4.68}$$

The above set of equations is sufficient if the baths are connected only at the terminal sites of the ladder.

Choose $j = 2N$ for the site at which the right bath is connected. Clearly, j is even. Therefore, we have the equations, in matrix form as:

$$\begin{pmatrix} \langle 3|T^{-N}|3\rangle & \langle 3|T^{-N}|4\rangle \\ \langle 4|T^{-N}|3\rangle & \langle 4|T^{-N}|4\rangle \end{pmatrix} \begin{pmatrix} \langle 1|M^{-1}|2N\rangle \\ \langle 2|M^{-1}|2N\rangle \end{pmatrix} = \begin{pmatrix} \frac{\langle 3|T^{-1}|2\rangle}{t_2} \\ \frac{\langle 4|T^{-1}|2\rangle}{t_2} \end{pmatrix} \tag{4.69}$$

$$\begin{pmatrix} \langle 1|M^{-1}|2N\rangle \\ \langle 2|M^{-1}|2N\rangle \end{pmatrix} = \begin{pmatrix} \langle 3|T^{-N}|3\rangle & \langle 3|T^{-N}|4\rangle \\ \langle 4|T^{-N}|3\rangle & \langle 4|T^{-N}|4\rangle \end{pmatrix}^{-1} \begin{pmatrix} \frac{\langle 3|T^{-1}|2\rangle}{t_2} \\ \frac{\langle 4|T^{-1}|2\rangle}{t_2} \end{pmatrix} \tag{4.70}$$

$$T^{-1} = \begin{pmatrix} 0 & 0 & 1 & 0 \\ 0 & 0 & 0 & 1 \\ -1 & 0 & -\frac{\mu}{t_1} & -\frac{t_r}{t_1} \\ 0 & -1 & -\frac{t_r}{t_2} & -\frac{\mu}{t_2} \end{pmatrix} \tag{4.71}$$

This gives:

$$\langle 1|M^{-1}|2N\rangle = \frac{\langle 3|T^{-N}|4\rangle}{t_2(\langle 3|T^{-N}|3\rangle \langle 4|T^{-N}|4\rangle - \langle 3|T^{-N}|4\rangle \langle 4|T^{-N}|3\rangle)} \tag{4.72}$$

$$\langle 2|M^{-1}|2N\rangle = \frac{-\langle 3|T^{-N}|3\rangle}{t_2(\langle 3|T^{-N}|3\rangle \langle 4|T^{-N}|4\rangle - \langle 3|T^{-N}|4\rangle \langle 4|T^{-N}|3\rangle)} \tag{4.73}$$

4.3.2 Ladder in presence of gauge field

For this case, we follow a nearly similar procedure. We find that the equation analogous to Eq. 4.55 is:

$$T(\mu)V_i(j) = V_{i-2}(j) - \frac{\delta_{i,j}|\mathbf{1}\rangle}{J^{\parallel}\exp\{i\phi/2\}} - \frac{\delta_{i+1,j}|\mathbf{2}\rangle}{J^{\parallel}\exp\{-i\phi/2\}} \tag{4.74}$$

Therefore, we notice that we can essentially replace, t_1 by $J^{\parallel}\exp\{i\phi/2\}$ and t_2 by $J^{\parallel}\exp\{-i\phi/2\}$, and all the calculations will remain valid till Eq. 4.70, and we will get:

$$\begin{pmatrix} \langle 1|M^{-1}|2N\rangle \\ \langle 2|M^{-1}|2N\rangle \end{pmatrix} = \begin{pmatrix} \langle 3|T^{-N}|3\rangle & \langle 3|T^{-N}|4\rangle \\ \langle 4|T^{-N}|3\rangle & \langle 4|T^{-N}|4\rangle \end{pmatrix}^{-1} \begin{pmatrix} \frac{\langle 3|T^{-1}|2\rangle}{J^{\parallel}\exp\{-i\phi/2\}} \\ \frac{\langle 4|T^{-1}|2\rangle}{J^{\parallel}\exp\{-i\phi/2\}} \end{pmatrix} \tag{4.75}$$

Finally, we get:

$$\langle 1|M^{-1}|2N\rangle = \frac{\langle 3|T^{-N}|4\rangle\, e^{-i\phi}}{J^{\parallel}e^{-i\phi/2}(\,\langle 3|T^{-N}|3\rangle\,\langle 4|T^{-N}|4\rangle - \langle 3|T^{-N}|4\rangle\,\langle 4|T^{-N}|3\rangle)} \tag{4.76}$$

$$\langle 2|M^{-1}|2N\rangle = \frac{-\langle 3|T^{-N}|3\rangle\, e^{-i\phi}}{J^{\parallel}e^{-i\phi/2}(\,\langle 3|T^{-N}|3\rangle\,\langle 4|T^{-N}|4\rangle - \langle 3|T^{-N}|4\rangle\,\langle 4|T^{-N}|3\rangle)} \tag{4.77}$$

4.4 Properties of the Green's function for the ladder

For both the cases- asymmetric hopping ladder and gauge field ladder, it is observed that if we reflect one of the bands about $E = 0$ (or about $E = V$ if there is a non-zero onsite potential V) and then do a translation of k by π, then we obtain the other band.

Therefore, mathematically,

$$\varepsilon^{+}(k) = -\varepsilon^{-}(k+\pi) \tag{4.78}$$

Now, for a ladder, we have:

$$G(\mu) = (\mu\mathbb{1} - H - \Sigma_s - \Sigma_d)^{-1} \tag{4.79}$$

For the time being let's ignore the self-energy terms. Then we have:

$$G(\mu) = \sum_k \frac{|\phi_k^{+}\rangle\langle\phi_k^{+}|}{\mu - \varepsilon^{+}(k)} + \sum_k \frac{|\phi_k^{-}\rangle\langle\phi_k^{-}|}{\mu - \varepsilon^{-}(k)} \tag{4.80}$$

Now, suppose we are interested in $G_{1,2N}(\mu)$, because baths are connected at the two extremes on different legs. We want to show $G_{1,2N}(\mu) = G_{1,2N}(-\mu)$. We'll see that this would be true in

general for any component of Green's function, and hence, $G(\mu) = G(-\mu)$.

$$\langle 1|G(\mu)|2N\rangle = \sum_k \frac{\langle 1|\phi_k^+\rangle\langle\phi_k^+|2N\rangle}{\mu-\varepsilon^+(k)} + \sum_k \frac{\langle 1|\phi_k^-\rangle\langle\phi_k^-|2N\rangle}{\mu-\varepsilon^-(k)} \tag{4.81}$$

$$\langle 1|G(\mu)|2N\rangle = \sum_k \frac{pq^*\exp\{-(N-1)ik\}}{\mu-\varepsilon^+(k)} + \sum_k \frac{p'q'^*\exp\{-(N-1)ik\}}{\mu-\varepsilon^-(k)} \tag{4.82}$$

A subtle thing to note is that p, p', q, q' are all themselves dependent on k because when k changes, so do the energies, which is used to determine the relation between p and q. Therefore, we can't pull them out of the summation sign.

Now, suppose N is even. If N is even, if we replace k with $k+\pi$, the set of k over which we are summing won't change. Since p, q (and p', q') depend on k, it can be shown that when $k \to k+\pi$, then $pq^* \to -p'q'^*$ and $p'q'^* \to -pq^*$.

$$\langle 1|G(\mu)|2N\rangle = \sum_k \frac{-p'q'^*\exp\{-(N-1)i(k+\pi)\}}{\mu-\varepsilon^+(k+\pi)} + \sum_k \frac{-pq^*\exp\{-(N-1)i(k+\pi)\}}{\mu-\varepsilon^-(k+\pi)} \tag{4.83}$$

$$\langle 1|G(\mu)|2N\rangle = \sum_k \frac{-p'q'^*(-1)\exp\{-(N-1)ik\}}{\mu+\varepsilon^-(k)} + \sum_k \frac{-pq^*(-1)\exp\{-(N-1)ik\}}{\mu+\varepsilon^+(k)} \tag{4.84}$$

$$\langle 1|G(\mu)|2N\rangle = \sum_k \frac{-p'q'^*\exp\{-(N-1)ik\}}{-\mu-\varepsilon^-(k)} + \sum_k \frac{-pq^*\exp\{-(N-1)ik\}}{-\mu-\varepsilon^+(k)} \tag{4.85}$$

$$\langle 1|G(\mu)|2N\rangle = -\left(\sum_k \frac{pq^*\exp\{-(N-1)ik\}}{-\mu-\varepsilon^+(k)} + \sum_k \frac{p'q'^*\exp\{-(N-1)ik\}}{-\mu-\varepsilon^-(k)}\right) \tag{4.86}$$

$$= -\langle 1|G(-\mu)|2N\rangle \tag{4.87}$$

Now, as a consequence of the above, consider $\mu = 0$. Then we find that:

$$\langle 1|G(0)|2N\rangle = -\langle 1|G(0)|2N\rangle \tag{4.88}$$

$$\implies \langle 1|G(0)|2N\rangle = 0 \tag{4.89}$$

Now, suppose we had baths connected on the p leg's extremes; then we'll have everything the same except, instead of pq^* (and $p'q'^*$), we'll have $pp* = |p|^2$ (and $|p'|^2$) as factors.

Now, if the self-energy terms are included, at least numerically, as far as I could check, the conductance is still equal for $\pm\mu$. Therefore, this needs to be confirmed and established more strongly.

It was also observed numerically that if the baths are placed at extremes but on different legs, it gives the same conductance for both the ways in which this can be done. Similarly, and perhaps more surprisingly, this was also observed when both the baths were on one leg. This claim needs to be proven and verified more rigorously, as numerically some very small deviations were observed. The following is a rough proof showing the connection between the two geometries that exist when baths are connected to different legs.

Assume N to be even. Then, we have:

$$\langle 2|G(\mu)|2N-1\rangle = \sum_k \frac{qp^* \exp\{-(N-1)ik\}}{\mu-\varepsilon^+(k)} + \sum_k \frac{q'p'^* \exp\{-(N-1)ik\}}{\mu-\varepsilon^-(k)} \tag{4.90}$$

Now, do the transformation $k \to -k$. Then, because of time reversal symmetry, $\varepsilon^{\pm}(k) = \varepsilon^{\pm}(-k)$. Therefore, we have:

$$\langle 2|G(\mu)|2N-1\rangle = \sum_k \frac{qp^* \exp\{(N-1)ik\}}{\mu-\varepsilon^+(-k)} + \sum_k \frac{q'p'^* \exp\{(N-1)ik\}}{\mu-\varepsilon^-(-k)} \tag{4.91}$$

$$\langle 2|G(\mu)|2N-1\rangle = \sum_k \frac{qp^* \exp\{(N-1)ik\}}{\mu-\varepsilon^+(k)} + \sum_k \frac{q'p'^* \exp\{(N-1)ik\}}{\mu-\varepsilon^-(k)} \tag{4.92}$$

$$\langle 2|G(\mu)|2N-1\rangle = \left(\sum_k \frac{pq^* \exp\{-(N-1)ik\}}{\mu-\varepsilon^+(k)} + \sum_k \frac{p'q'^* \exp\{-(N-1)ik\}}{\mu-\varepsilon^-(k)} \right)^* \tag{4.93}$$

$$\implies \langle 2|G(\mu)|2N-1\rangle = \langle 1|G(\mu)|2N\rangle^* \tag{4.94}$$

4.5 Numerical Results

In what follows, the numerical calculations were done with the baths connected at extremes, either on different or on the same leg. A wide band limit is taken for the baths, making the self-energy

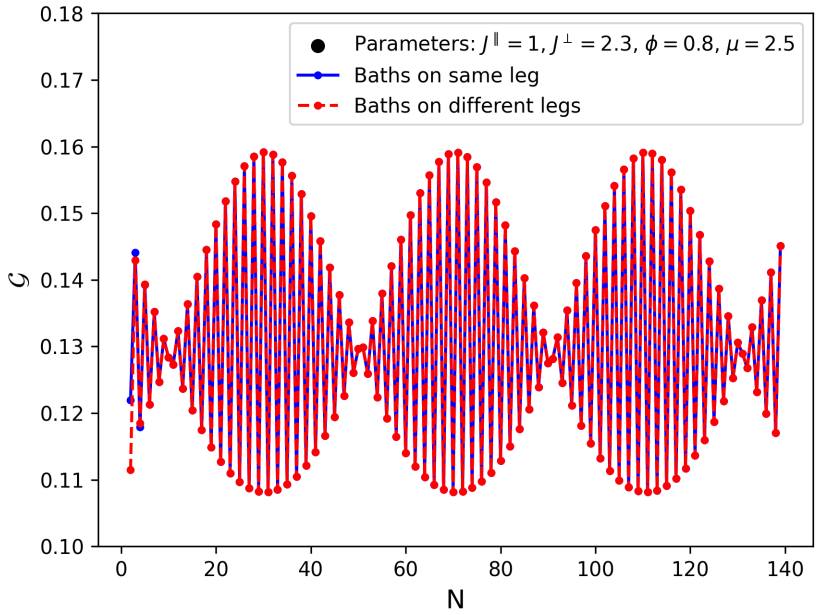

Figure 4.5: Ballistic behavior in a gauge field ladder because the chemical potential μ cuts through the band

matrix have a non-zero constant diagonal value at the sites where baths are connected. Unless otherwise stated, it has $-i$ as its first and last diagonal element, with all other elements at zero. Also, $J^{\parallel}$ is taken to be 1, unless stated otherwise.

Ballistic regime:

This was observed whenever the $\varepsilon = \mu$ cuts any of the bands. Singularities (or very large conductance values) were observed without the self-energy terms, but adding the self-energy terms made the conductance bounded. This is shown in Fig. 4.5. **Subdiffusive regime ($1/N^2$ scaling):**

This was observed when μ corresponds to band edges (single 2nd order EP or 4th order EP) without intersecting any of the band. This is shown in Fig. 4.6. **Oscillating Subdiffusive regime:**

In the vortex regime, we find the existence of 2 second-order EPs at the extreme band edges. The k difference between them is between π and 2π, and hence, they show an overall subdiffusive scaling of $1/N^2$ but with oscillations.

Interestingly, the oscillations are greater when the bath is connected to different legs. This is

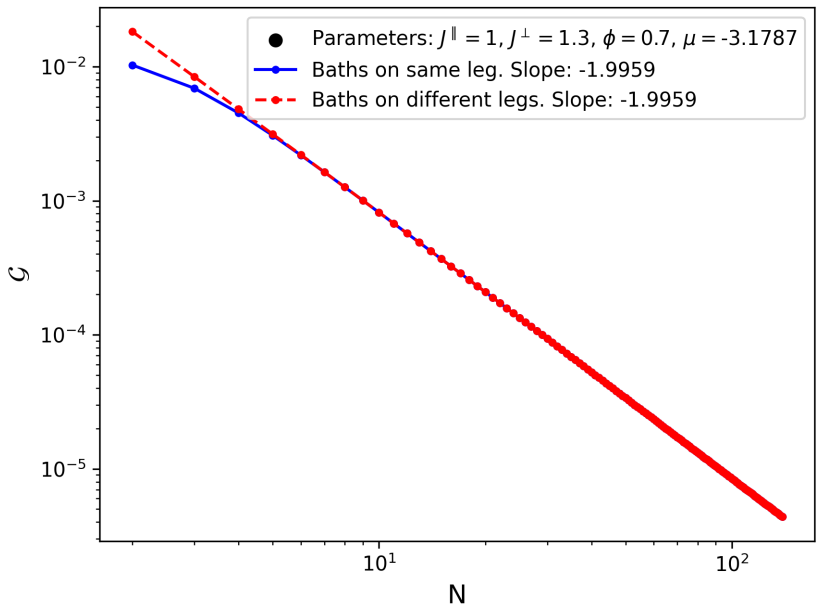

Figure 4.6: Conductance showing $1/N^2$ scaling corresponding to a band edge without intersecting the band, with the extrema at $k = \pi$

precisely why the scaling is slightly different from $1/N^2$. This is shown in Fig. 4.7.

The oscillations are caused due to the complex nature of the eigenvalues of the Transfer matrix.

Localized regime:

An exponential decay of conductance is observed with N when μ doesn't intersect any of the bands, and we are in the Meissner regime. This is shown in Fig. 4.8.

Oscillating Localized regime:

This is the analogous localized transport for the vortex regime. Interestingly, there are negligible or no fluctuations when baths are connected on the same leg. This is shown in Fig. 4.9.

These oscillations seem to occur generally, even for the Meissner regime when μ is in the localized regime (and sufficiently large so that the eigenvalues become complex-valued). So, the Meissner regime is different from the Vortex regime because there exists a window wherein one gets real eigenvalues in the localized regime. The above claim is based on observations for test

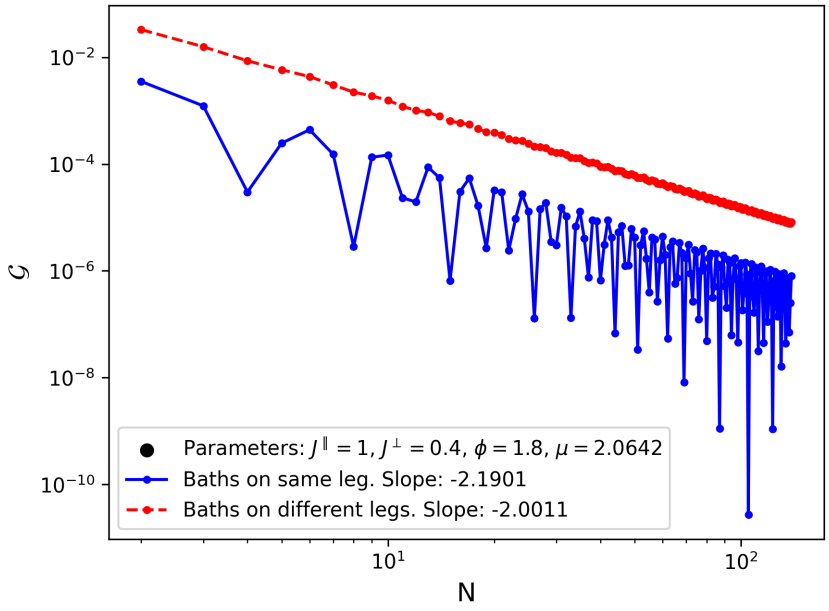

Figure 4.7: Conductance showing $1/N^2$ scaling with oscillations corresponding to a band edge without intersecting the band, with the extrema between $k = 0$ and $k = \pi$, leading to complex eigenvalues of the transfer matrix.

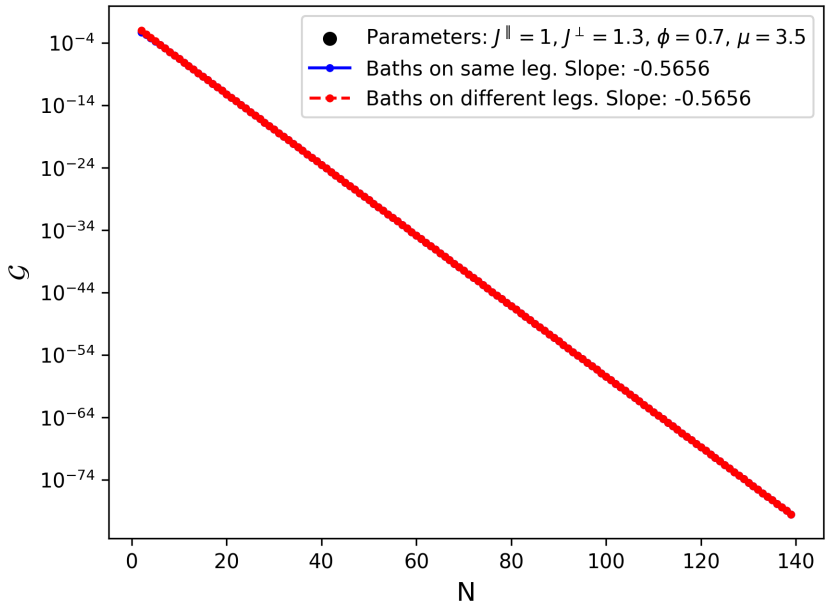

Figure 4.8: The conductance is exponentially localized because the chemical potential is outside the bandwidth.

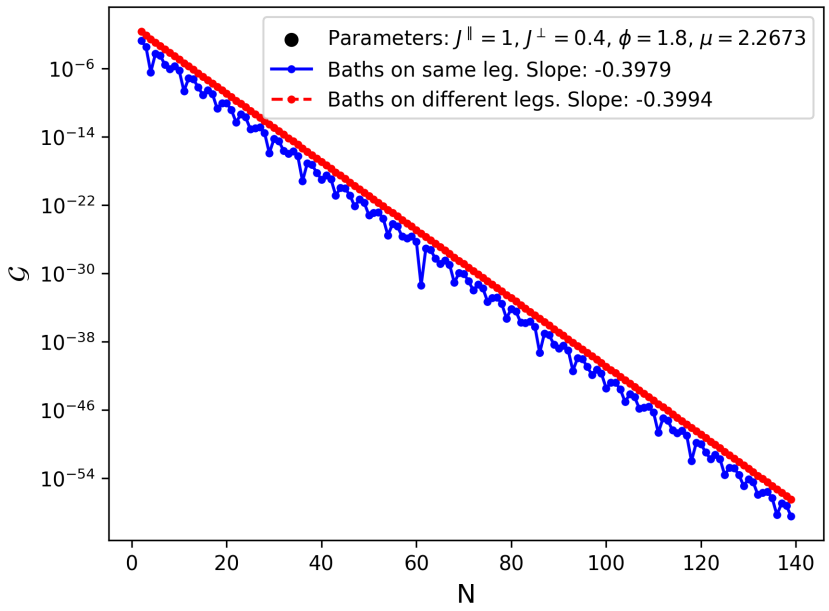

Figure 4.9: This shows a localized regime with fluctuations, primarily when baths are connected on the same leg. This happens due to the complex nature of eigenvalues, with more details in the text.

cases and needs to be proved properly.

Special cases:

$\mu = 0$: For this case, the conductance goes to zero for even N when baths are connected across and for odd N when baths are connected on the same side, for any value of other parameters. Note that for the gapped-ungapped phase separating line, $\mu = 0$ also serves as a band edge for both the upper and lower band, and hence, one sees the subdiffusive ($\sim 1/N^2$ scaling of conductance). All the regimes are shown in Fig. 4.10, 4.11 and 4.12

$\phi = \pi$: For this case, the two second-order exceptional points occur at $k = \pm\pi/2$. Here, the lower band is just the reflection of the upper band about the x-axis. When the baths are connected on different legs, this leads to a vanishing conductance for even N for any arbitrary values of other parameters. This is shown in Fig. 4.13.

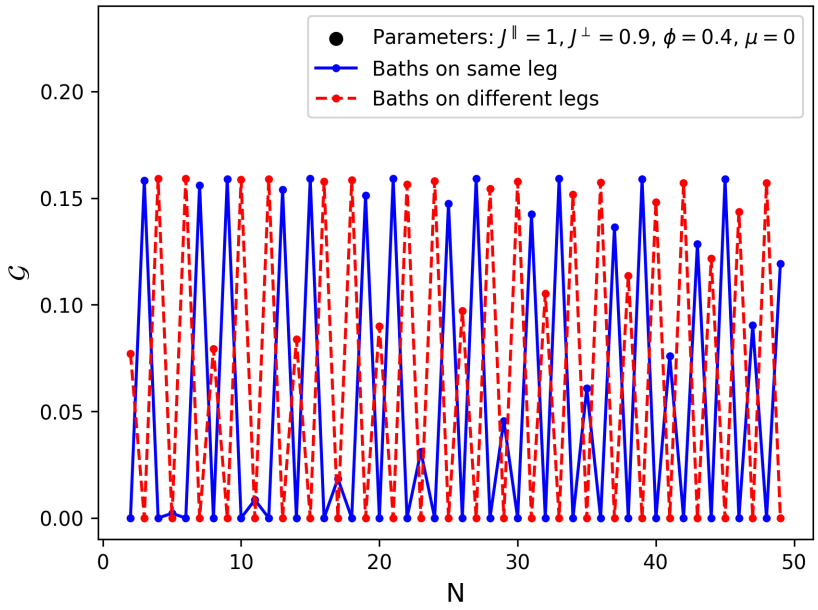

Figure 4.10: Ballistic conductance with $\mu = 0$, vanishing based on odd or even no. of sites.

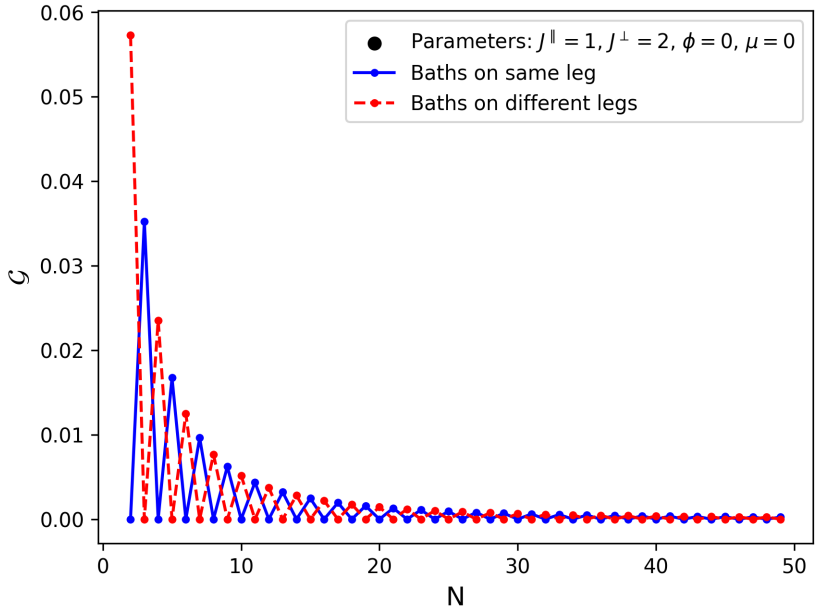

Figure 4.11: Subdiffusive $1/N^2$ scaling of conductance with $\mu = 0$, vanishing based on odd or even no. of sites.

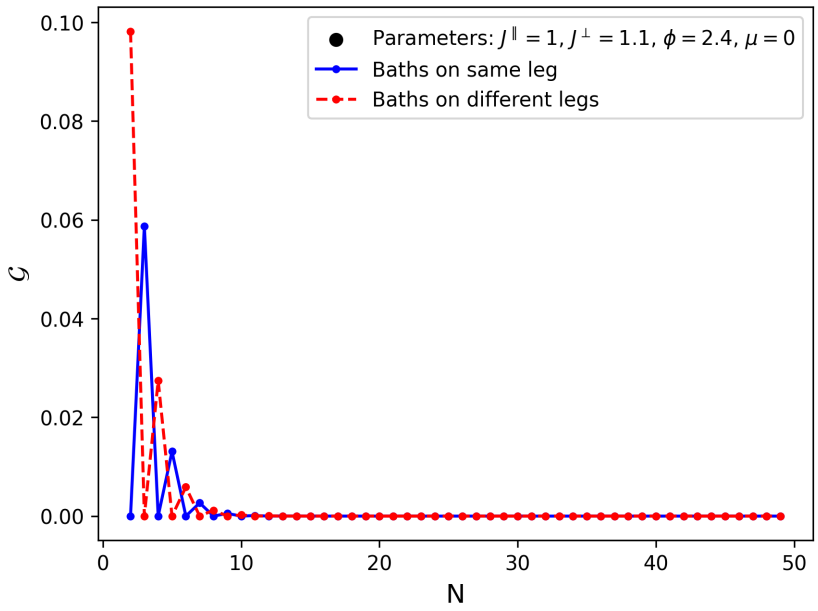

Figure 4.12: Exponentially localized conductance with $\mu = 0$, vanishing based on odd or even no. of sites.

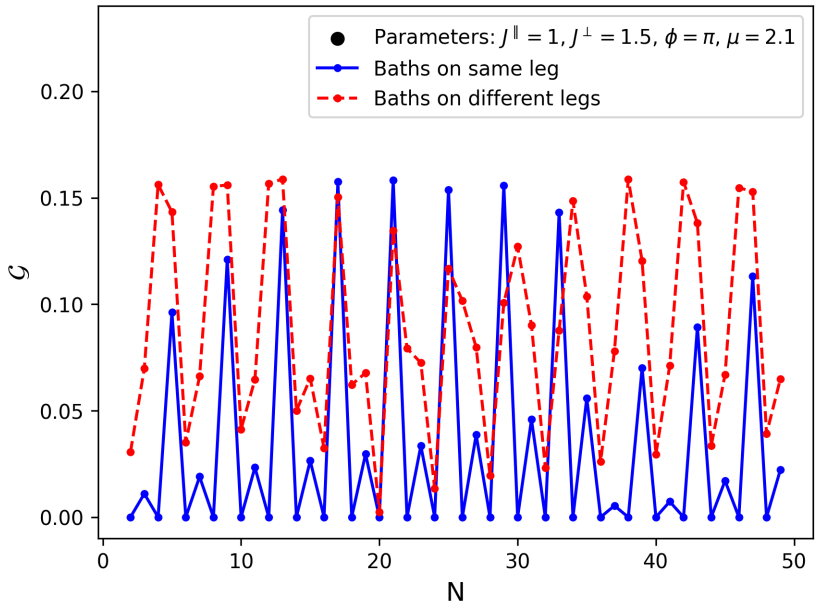

Figure 4.13: Ballistic conductance with $\phi = \pi$, vanishing based on odd or even no. of sites for baths connected on the same leg, while no special transport for baths connected on different legs.

Chapter 5

Conclusion and Outlook

We studied quantum transport in a one-dimensional lattice system hosting long-range power-law decaying hopping with inelastic scattering. An anomalous super-diffusive scaling is obtained in a long-range parameter regime via two approaches. The first is an exact method using Landauer-Buttiker formalism to study a boundary-driven lattice with Buttiker probes attached at each site mimicking dephasing. The second method uses the Lindblad equation to model the dephasing probes and study wavepacket dynamics. It is interesting to see the agreement between these methods and it suggests a universality in the strong probe coupling regime. The fractional diffusion equation describing the super-diffusive transport is microscopically derived using the renormalisation technique, and the scaling exponents and scaling functions are compared analytically and numerically. This opens up several prospects, like determining the stability of scaling in the presence of weak interactions, investigating the universality class to which our model belongs, etc. Also, one could attempt to apply similar techniques to predict hydrodynamic transport for other models.

We move on to study fermionic transport in boundary-driven quasi one-dimensional ladder models. Transfer matrix techniques prove very useful in obtaining analytically tractable forms for conductance. Exceptional points of the matrix are shown to correspond to phase boundaries for a simple

ladder in a gauge field. We report some special parameter values for which conductance shows dependence on the system size being odd or even and the placement of the boundary baths. Symmetries of the model are argued to be the reason behind this. There is a possibility of generalizing the models to two dimensions in an appropriate manner.

In summary, we have investigated quantum transport in non-interacting one-dimensional and quasi one-dimensional systems. We have found some interesting transport phenomena which open up exciting future possibilities.

Bibliography

[1] C. Maier, T. Brydges, P. Jurcevic, N. Trautmann, C. Hempel, B.P. Lanyon et al., *Environment-assisted quantum transport in a 10-qubit network*, *Phys. Rev. Lett.* **122** (2019) 050501.

[2] F. Caruso, A.W. Chin, A. Datta, S.F. Huelga and M.B. Plenio, *Highly efficient energy excitation transfer in light-harvesting complexes: The fundamental role of noise-assisted transport*, *The Journal of Chemical Physics* **131** (2009) .

[3] M. Saha, B.P. Venkatesh and B.K. Agarwalla, *Quantum transport in quasiperiodic lattice systems in the presence of B\"uttiker probes*, *Phys. Rev. B* **105** (2022) 224204.

[4] A. Dhar, A. Kundu and A. Kundu, *Anomalous Heat Transport in One Dimensional Systems: A Description Using Non-local Fractional-Type Diffusion Equation*, *Front. Phys.* **7** (2019) .

[5] Y. Meir and N.S. Wingreen, *Landauer formula for the current through an interacting electron region*, *Phys. Rev. Lett.* **68** (1992) 2512.

[6] A. Dhar and D. Sen, *Nonequilibrium Green's function formalism and the problem of bound states*, *Phys. Rev. B* **73** (2006) 085119.

[7] A. Purkayastha, M. Saha and B.K. Agarwalla, *Subdiffusive Phases in Open Clean Long-Range Systems*, *Phys. Rev. Lett.* **127** (2021) 240601.

[8] H. Haug, A.-P. Jauho et al., *Quantum kinetics in transport and optics of semiconductors*, vol. 2, Springer (2008).

[9] M. Saha, B.K. Agarwalla, M. Kulkarni and A. Purkayastha, *Universal Subdiffusive Behavior at Band Edges from Transfer Matrix Exceptional Points*, *Phys. Rev. Lett.* **130** (2023) 187101.

[10] W.D. Heiss, *The physics of exceptional points*, *J. Phys. A: Math. Theor.* **45** (2012) 444016.

[11] M. Saha, B.K. Agarwalla, M. Kulkarni and A. Purkayastha, *Environment assisted superballistic scaling of conductance*, *Phys. Rev. B* **108** (2023) L161115.

[12] W.M. Itano, D.J. Heinzen, J.J. Bollinger and D.J. Wineland, *Quantum zeno effect*, *Physical Review A* **41** (1990) 2295.

[13] S. Sarkar, B.K. Agarwalla and D.S. Bhakuni, *Impact of dephasing on non-equilibrium steady-state transport in fermionic chains with long-range hopping*, Oct., 2023. 10.48550/arXiv.2310.01323.

[14] A. Purkayastha, S. Sanyal, A. Dhar and M. Kulkarni, *Anomalous transport in the Aubry-Andr\'e-Harper model in isolated and open systems*, *Phys. Rev. B* **97** (2018) 174206.

[15] D.S. Bhakuni, T.L.M. Lezama and Y.B. Lev, *Noise-induced transport in the Aubry-Andr\'e-Harper model*, July, 2023. 10.48550/arXiv.2307.06373.

[16] T. LM Lezama and Y. Bar Lev, *Logarithmic, noise-induced dynamics in the anderson insulator*, *SciPost Physics* **12** (2022) 174.

[17] X. Turkeshi and M. Schiró, *Diffusion and thermalization in a boundary-driven dephasing model*, *Phys. Rev. B* **104** (2021) 144301.

[18] M. Esposito and P. Gaspard, *Emergence of diffusion in finite quantum systems*, *Phys. Rev. B* **71** (2005) 214302.

[19] L.-Y. Chen, N. Goldenfeld and Y. Oono, *Renormalization group and singular perturbations: Multiple scales, boundary layers, and reductive perturbation theory*, *Phys. Rev. E* **54** (1996) 376.

[20] K. Fujimoto, R. Hamazaki and Y. Kawaguchi, *Impact of Dissipation on Universal Fluctuation Dynamics in Open Quantum Systems*, *Phys. Rev. Lett.* **129** (2022) 110403.

[21] A. Schuckert, I. Lovas and M. Knap, *Nonlocal emergent hydrodynamics in a long-range quantum spin system*, *Phys. Rev. B* **101** (2020) 020416.

[22] M.K. Joshi, F. Kranzl, A. Schuckert, I. Lovas, C. Maier, R. Blatt et al., *Observing emergent hydrodynamics in a long-range quantum magnet*, *Science* **376** (2022) 720.

[23] A. Dhar, K. Saito and B. Derrida, *Exact solution of a L\'evy walk model for anomalous heat transport*, *Phys. Rev. E* **87** (2013) 010103.

[24] S. Iubini, S. Lepri and S. Ruffo, *Hydrodynamics and transport in the long-range-interacting 4 chain*, *J. Stat. Mech.* **2022** (2022) 033209.

[25] M. Saha and S.K. Maiti, *Particle current rectification in a quasi-periodic double-stranded ladder*, *J. Phys. D: Appl. Phys.* **52** (2019) 465304.

[26] R.A. Silva and M. Almeida, *Spin-ladder behaviour in molecular materials*, *Journal of Materials Chemistry C* **9** (2021) 10573.

[27] B. Xing, X. Xu, V. Balachandran and D. Poletti, *Heat, particle, and chiral currents in a boundary driven bosonic ladder in the presence of a gauge field*, *Phys. Rev. B* **102** (2020) 245433.

[28] Y.-J. Zhao, X.-W. Xu, H. Wang, Y.-x. Liu and W.-M. Liu, *Vortex-Meissner phase transition induced by a two-tone-drive-engineered artificial gauge potential in the fermionic ladder constructed by superconducting qubit circuits*, *Phys. Rev. A* **102** (2020) 053722.

[29] M. Saha, M. Kulkarni and B.K. Agarwalla, *Exceptional hypersurfaces of transfer matrices of finite-range lattice models and their consequences on quantum transport properties*, *Phys. Rev. B* **108** (2023) 075406.